The Role of Intramolecular Relaxations on the Structure and Stability of Vapor-Deposited Glasses

Aixi Zhang,^{1, a)} Alex R. Moore,^{1, 2, a)} Haoqiang Zhao,¹ Shivajee Govind,¹ Sarah E. Wolf,¹ Yi Jin,¹ Patrick J. Walsh,¹ Robert A. Riggleman,^{2, b)} and Zahra Fakhraai^{1, b)}

1) Department of Chemistry, University of Pennsylvania, Philadelphia, Pennsylvania,
19104

Stable glasses (SGs) are formed through surface-mediated equilibration (SME) during physical vapor deposition (PVD). Unlike intermolecular interactions, the role of intramolecular degrees of freedom in this process remain unexplored. Here, using experiments and coarse-grained molecular dynamics simulations, we demonstrate that varying dihedral rotation barriers of even a single bond, in otherwise isomeric molecules, can strongly influence the structure and stability of PVD glasses. These effects arise from variations in the degree of surface mobility, mobility gradients, and mobility anisotropy, at a given deposition temperature (T_{dep}) . At high T_{dep} , flexible molecules have access to more configurations, which enhances the rate of SME, forming isotropic SGs. At low T_{dep} , stability is achieved by out of equilibrium aging of the surface layer. Here, the poor packing of rigid molecules enhances the rate of surface-mediated aging (SMA), producing stable glasses with layered structures in a broad range of T_{dep} . In contrast, the dynamics of flexible molecules couple more efficiently to the glass layers underneath, resulting in reduced mobility and weaker mobility gradients, producing unstable glasses. Independent of stability, the flattened shape of flexible molecules can also promote in-plane orientation order at low T_{dep} . These results indicate that small changes in intramolecular relaxation barriers can be used as an approach to independently tune the structure and mobility profiles of the surface layer and thus the stability and structure of PVD glasses.

Keywords: Stable Glass, Surface-Mediated Equilibration, Surface Mobility, Dihedral Rotations, Glass Birefringence, Structural Anisotropy, Molecular Layering

²⁾Department of Chemical and Biomolecular Engineering, University of Pennsylvania, Philadelphia, PA 19104

^{a)}Equal contributions: These authors contributed equally to this work.

b)Corresponding Authors: fakhraai@sas.upenn.edu, rrig@seas.upenn.edu

I. INTRODUCTION

Stable glasses (SGs) are produced by physical vapor deposition (PVD) at relatively slow deposition rates onto substrates held below the glass transition temperature (T_g) of the material $^{1-5}$. Since their discovery 1 , stable glasses made of organic molecules have been studied extensively and shown to have improved density 3,6 and thermal stability 1,2,4,7,8 , analogous to highly-aged liquid quenched glasses (LQG). Vapor-deposited glasses also exhibit various degrees of optical birefringence $^{6,9-14}$, magnetic anisotropy 15 , and structural anisotropy $^{12,16-23}$. Stability and structural ansiotropy are critical factors in tuning the optical 9,21,24 , mechanical $^{25-28}$, and electronic 17,29,30 properties of organic thin films in applications such as coatings and functional devices. As such, it is essential to understand the interplay between structural anisotropy and glass stability, as the molecular structure and deposition conditions are varied.

Structural anisotropy in PVD glasses is predominantly due to two factors; preferred molecular orientation 18,20,31 and molecular layering 16,23,32 . In general, when vapor-deposition is performed at low deposition temperatures (T_{dep}), a preferred in-plane orientation is observed for both rod-like and disc-like molecules 20 , resulting in negative optical birefringence. At intermediate T_{dep} , out-of-plane orientation is observed for elongated molecules 12 with positive optical birefringence. Deposition close to T_g^{33} , at slow deposition rates (r_{dep}) 34 , or for molecules with smaller aspect ratios, results in isotropic packing 35 . Both experiments and simulations indicate that the origins of this orientational anisotropy lies in the structure of the supercooled liquid at or close to the free surface 10,12,34,36 .

Molecular layering, in the direction normal to the substrate surface, is also a ubiquitous feature of vapor-deposited glasses 16,23,32 but its origins are not well understood. In wide-angle X-ray scattering (WAXS) experiments, layering is observed as a distinct scattering peak in the out-of-plane scattering direction 16,18,32 . This peak is observed even in molecules that are isotropic and do not adopt preferred orientations 32 , at a length scale that roughly corresponds to the molecule's size. We have previously shown that in vapor-deposited glasses of 9-(3,5-di(naphthalen-1-yl)phenyl)anthracene (α , α -A), the molecules adopt isotropic orientations due to their spherical shape, but still show a positive optical birefringence, which can only then arise due to tighter intermolecular distancing in the normal direction 23 . A strong correlation is observed between the out-of-plane index of refraction and density in these films, providing further evidence for tighter molecular packing in the direction normal to the free surface. We have hypothesized

that this phenomenon is also tied to molecular layering, and occurs due to out of equilibrium dynamics close to the free surface (*i.e.* physical aging) under constraint of a rigid substrate. As the molecules are buried upon continued vapor-deposition and fall out of equilibrium, they are influenced by the out of equilibrium stable glass beneath, which limits their mobility in the in-plane direction²³. Recent experiments have provided direct evidence of accelerated aging process in layers near the free surface of vapor-deposited glasses³⁷.

Making a distinction between surface-mediated equilibration (SME), where the surface relaxation dynamics are fast enough for the surface region to reach its own respective equilibrium state, vs. surface-mediated accelerated aging (SMA), where all or some portions of the surface layer are out of equilibrium but can still age at a rate faster than bulk, can provide some insight into these observations. Surface boundary conditions can dictate in-plane orientation at the immediate free surface of a supercooled liquid, while the layer directly below can take an out-of-plane orientation 10,35,38 or become isotropic a few layers below the free immediate surface 39. As such, the thickness of the mobile layer, at a given effective deposition rate, as well as mobility gradients that can enable accelerated aging, play a critical role in defining the orientational order of vapor-deposited glasses^{35,38}. During PVD, the thickness of the surface layer defines the depth at which the molecules are able to optimize their configuration, and reach their equilibrated liquid structure^{32,36,39,40}. While enhanced surface diffusion and relaxation have been ubiquitously observed on the surface of liquid-quenched^{41–45} and vapor-deposited molecular glasses^{46–48}, and have been shown to have a weak temperature dependence^{49–51}, measuring the depth of this mobile layer and its dynamical gradients are challenging and can be highly dependent on the material type and the range of relaxation times being probed^{34,37,52}. Experiments in polymeric glasses suggest that the thickness of the mobile layer sharply decreases from a 4-7 nm at T_g to ~ 1 nm around $0.9T_e^{53-55}$. A recent in situ study of vapor-deposited 2-methyltetrahydrofuran glasses estimated a 2.5 nm thickness for the mobile surface layer at $0.82T_g^{37}$, which is also consistent with results from molecular dynamics simulations ^{10,18,36,39,56}.

In this study, we investigate the role of barriers for dihedral rotations in otherwise isomeric molecules to elucidate the role of molecular shape and intramolecular degrees of freedom on the surface mobility and mobility gradients, and thus the structure and stability of vapor-deposited glasses. In experiments, we compare the properties of α , α -A with 9-(3,5-di(naphthalen-1-yl)phenyl)phenanthrene (α , α -Phen), by replacing the anthracene (-A) substituent with a phenanthrene (-Phen) group (structures shown in Figure 1A). This simple replacement, which preserves

the molecular weight and inter-molecular interactions, results in a reduction in the rotational barrier for the Phen-diarylbenzene bond compared to the A-diarylbenzene bond and changes the equilibrium shape of the molecule from spherical α , α -A to a more flattened ellipsoidal α , α -Phen. This structural change has a surprisingly large effect on the stability and structural anisotropy of α , α -Phen glasses deposited at low T_{dep} .

In simulations, coarse-grained models of these molecules show anisotropic relaxation dynamics at the mobile free surface, which change with varying intramolecular relaxations. These variations can explain how rotational barriers can influence the temperature dependence of mobility anisotropy and the range of mobility gradients of the surface layer, and their influence on the stability of simulated PVD glasses. Combined, these results demonstrate how mobility gradients can influence molecular orientation and layering, and thus elucidate the T_{dep} range which SGs are formed through surface-mediated equilibration vs. the regime where accelerated aging plays a role in the formation of anisotropic stable glasses.

II. MATERIALS AND METHODS

A. Experimental Details

Synthesis and sample preparation. 9-(3,5-di(naphthalen-1-yl)phenyl)anthracene (α , α -A) and 9-(3,5-di(naphthalen-1-yl)phenyl)phenyl)phenanthrene (α , α -Phen) were synthesized using Suzuki cross-coupling reactions and purified as detailed in our earlier publications^{57,58}. The structures of these compounds are shown in Figure 1A. Depending on the characterization method, films with thicknesses of $h \sim 24$ nm, $h \sim 150$ -240 nm, or $h \sim 1$ μ m were prepared by physical vapor deposition (PVD) using a custom high-vacuum chamber with a base pressure of $\sim 2 \times 10^{-7}$ Torr^{49,59,60}. Before deposition, each compound was pre-melted in a vacuum oven (Fisherbrand Isotemp 281A, $P \sim 1$ kPa) at ~ 543 K for α , α -A (melting point $T_{m,A} = 508 \pm 2$ K) and ~ 483 K for α , α -Phen ($T_{m,Phen} = 448 \pm 2$ K), respectively. The melting points were determined by differential scanning calorimetry (DSC, TA instruments Q2000). The compounds were vapor-deposited onto silicon substrates (Si(100) with native oxide, Virginia Semiconductor Inc.) that were mounted on a bridge between two temperature-controlled copper stages (Figure S1) to produce temperature-gradient (T-grad) samples, with a broad range of deposition temperatures (T_{dep}). Binder clips were used along with Apiezon PFPE 501 Thermal Grease (silicone-free, ultra-high vacuum), to ensure strong

thermal contact at each end. Details of the calibration and T_{dep} determination can be found in the supplementary information (SI and Figures S2-3) and our previous publications^{59,60}. The deposition rate (r_{dep}) was monitored using a quartz crystal microbalance (QCM, Inficon STM-2). A movable shutter placed about 2 cm above the crucible was used to ensure that the target rate of $r_{dep} = \pm 0.2$ Å/s was reached before the start of deposition and maintained throughout each deposition. After deposition, the temperature of the hot-side of each T-grad sample was rapidly quenched and the cold-side was heated to room temperature. Samples were removed and characterized by SE within an hour of deposition or were stored at 254 K for other characterizations.

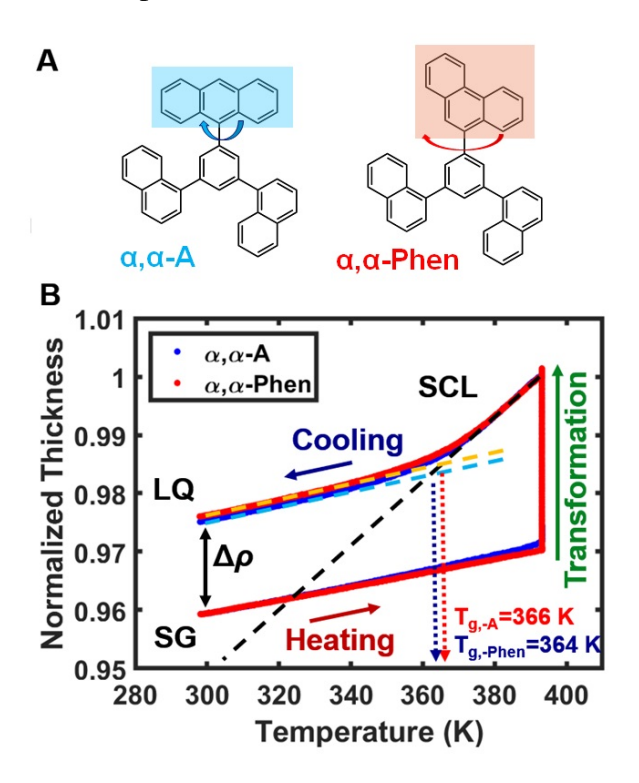


Figure 1. (A) The chemical structures of α , α -A (left) and α , α -Phen (right) molecules. The arrows show the dihedral rotations that are different in the two molecules. (B) Normalized thickness vs. temperature during the transformation cycle of \sim 240 nm PVD films of α , α -A (blue) and α , α -Phen (red) deposited at $T_{dep,A} = 301\pm4$ K and $T_{dep,phen} = 303\pm4$ K (\sim 0.83 T_g for both molecules). $\Delta \rho \simeq 1.5\pm0.1\%$ at 298 K (black arrow). Dashed lines represent linear fits to the SCL and liquid-quenched glass (LQG) regions for each film which is used to define the T_g values shown in the inset.

a. Spectroscopic Ellipsometry. Variable-angle spectroscopic ellipsometry (SE, Woollam M-2000 V) was used to obtain the film thickness and the in-plane (n_{xy}) and out-of-plane (n_z) indices of refraction as a function of T_{dep} by performing automatic multi-angle SE scans mapping a

 3×32 grid, with 0.2 cm distance between each measured point (details in the SI and our previous publications)^{59,60}. The optical properties of as-deposited PVD films were modeled using a transparent anisotropic Cauchy layer (details in the SI and Figures S4-S5). The indices of refraction were calculated at a wavelength of $\lambda = 632.8$ nm.

Due to the limitations of the sample size for the heating stage (Linkam temperature-controller, THMS600), after a first full SE scan at room temperature, as-deposited T-grad samples were split into three pieces, each about 2.8 cm in length. Each sample was subject to a thermal transformation cycle, by heating from 298 K to 393 K at 10 K/min, annealing at 393 K for 30 min, and subsequently cooling back to 298 K at 10 K/min to form the liquid-quenched glass (LQG). During each cycle, *in situ* SE measurements were performed at a single point on each sample to ensure that the sample was fully transformed, *i.e.* reaching a constant thickness at 393 K. Because micron-thick films are vulnerable to stress-induced crack formation during transformation, these experiments were only performed on films with thicknesses of $h \sim 150$ nm - 240 nm.

After each transformation cycle, multi-angle SE mapping was performed at room temperature (298 K) and the data was fitted as described above. The density change ($\Delta\rho$) was calculated at each grid point (T_{dep} value) by comparing the *ex situ* values of thickness obtained at the same coordinates before and after the transformation. An example of this data is shown in Figure 3A. Typically, three data points were collected at the same T_{dep} (along the width of the sample, *y*-direction) and the data was averaged to improve accuracy. The reported values of $\Delta\rho$ and indices of refraction are based on averaged values collected from several independent depositions (more details in the SI).

The glass transition temperatures (T_g s) of α , α -A and α , α -Phen were measured during *in situ* SE experiments upon cooling (Figure 1B) by fitting lines to the data in the range of 383 K to 393 K, for the supercooled liquid (SCL) regime, and 310 K to 330 K, for the glass regimes, respectively. T_g s were determined to be $T_{g,-A} = 364 \pm 1$ K and $T_{g,-Phen} = 366 \pm 1$ K, respectively. The thermal expansion coefficients of the two molecules in the SCL (α_{SCL}) and glass (α_{GL}) states were also determined based on the slopes of these lines and are reported in Table S1 of SI.

b. Dewetting experiments. Dewetting experiments were performed on thin films (h = 24 nm) by monitoring the evolution of their morphology using Atomic Force Microscopy (AFM, Agilent Technologies 5420, closed-loop scanner, N9524B). Each film's morphology was first measured at room temperature (298 K). The samples were then heated to the target annealing temperature using a thermoelectric setup (Custom Thermoelectric modules and Oven Industries

controller) and held isothermally. After 90 min, heating was turned off and the samples were allowed to cool to room temperature. The final morphology was collected within 10 min after the heating source was turned off.

c. Grazing incidence Wide-angle X-ray scattering. Grazing Incidence Wide-angle X-ray Scattering (GIWAXS) data were obtained at room temperature on $h \sim 1 \,\mu$ m samples using a Xeuss 2.0 X-ray scattering instrument (Xenocs), with a Cu K- α beam. The incident angle was set at 0.2° . Typically, 16 evenly-distributed points were measured on each T-grad sample at room temperature (more details in the SI and SI figures S7-S9). The data reported for each molecule, are based on the averaged values of two independent measurements on $1 \,\mu$ m samples, and the vertical error bars show the standard error of these measurements. The horizontal error bars for defining T_{dep} were obtained based on T-grad calibration and positioning errors (details in the SI).

B. Simulations and Modeling

a. Density Functional Calculations. Density Functional Theory (DFT) calculations were performed using Gaussian on WebMO with B3LYP functional and 6-31G(d) basis. First, the molecular geometry of α , α -A and α , α -Phen were optimized. These optimized geometries are shown in Figure 2A (more detailed representation shown in SI Figure S10) As shown in this Figure, The optimized dihedral angles around the anthracene-3,5-di(naphthalen-1-yl)benzene (A-diarylbenzene) bond and phen-diarylbenzene bonds are measured to be -89.8° and -56.6°, respectively. As such, α , α -A is more spherical in shape, while α , α -Phen has a flattened elliptical shape. The dimensions of α , α -A are estimated to be \sim 1.2 nm at all direction. For α , α -Phen, the molecule's short axes are \sim 1.2 nm while its long axis is \sim 1.4 nm (Figures 2A).

Coordination scans were then performed on the dihedral angles of the A-diarylbenzene and Phen-diarylbenzene bonds between -180° to 180°. At each step, the anthracene/phenanthrene moiety were rotated with a step size of either 10° away from the energy barrier or 1° close to the maximum energy barrier. The molecular geometry was optimized after each rotation and the molecular energy was calculated under the constrain of a fixed dihedral angle. More details of these calculations can be found in the SI and Figure S10. Based on these calculations, the dihedral rotation barrier for the Phen-diarylbenzene bond in α , α -Phen and the A-diarylbenzene bond in α , α -A were estimated to be \sim 13 kcal/mol and \sim 20 kcal/mol, respectively. The estimated barrier for the A-diarylbenzene bond is consistent with previous measurements⁶¹ and ab-initio

simulations⁶² in other organic molecules.

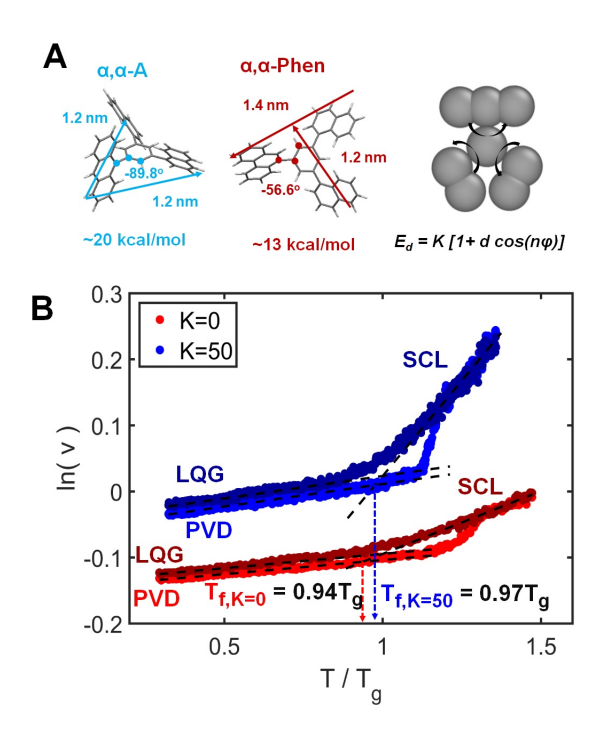


Figure 2. (A) The equilibrium structures of α , α -A (left) and α , α -Phen (middle), calculated by DFT, and the coarse-grained model molecule (right) used in the MD simulations. The black arrows show the dihedral rotations that are varied in the MD simulations, with the dihedral rotation barriers listed below each molecule. E_d shows the barrier for the model molecule. The K value was either set to K=0 (a more flexible version of α , α -Phen) or K=50 (a more rigid version of α , α -A). (B) Natural logarithm of the specific volume (ln(V)) vs. normalized temperature (T/T_g) during transformation of simulated films with K=0 (red) and K=50 (blue) deposited at $T_{dep}=0.87T_g$. Dashed lines represent linear fits to the SCL and LQG regions to measure T_g and T_f . $T_{f,K=0}=0.94T_g$ for K=0, and $T_{f,K=50}=0.97T_g$, for K=50 molecules, respectively.

b. Coarse-Grained Molecular Dynamics Simulations. The simulated vapor deposition process was adopted from the process used in our previous studies^{39,63}. Molecular dynamics simulations were performed using the LAMMPS⁶⁴ package in the NVT ensemble with a time step of 0.002. A coarse-grained molecular model was constructed based on α , α -A, using eight interconnected Lennard-Jones (LJ) particles, each with parameters $\sigma = 1.0$ and $\varepsilon = 1.0$. The LJ potential used here includes a cutoff distance at $r_c = 2.5$ and decays smoothly to zero. Harmonic bonds (7 per molecule, $l_{bond} = 1.0, 0.667, K_{bond} = 500$) and angles (8 per molecule, $\theta_{angle} = 1.0$).

 90° , 120° , 180° , $K_{\rm angle} = 100$) were used to create the general shape and structure of the molecule. Additionally, harmonic dihedral potentials ($E_d = K[1 + d\cos(n\phi)]$) were implemented between groups of four particles representing the side groups of the molecule (4 per molecule, d = +1, n = 1) and the strength of this harmonic dihedral potential was varied as the parameter controlling the rigidity of the molecule in these studies (K = 0, 50). The simulation box was chosen to be $15\sigma \times 15\sigma$ in the x - y plane and was long enough in the z direction to always allow at least 10σ of vacuum space above the free surface of the PVD film. PVD was emulated by performing approximately 2000 single molecule deposition cycles, where a cycle consisted of (1) introducing a new, randomly oriented molecule above the film free surface, (2) linear cooling of the molecule from the high temperature, $T = 1.4T_g$, to T_{dep} , and (3) minimizing the energy of the system. Each molecule was allowed 150τ , where τ is the standard LJ time unit, from time of introduction to the end of this linear cooling, analogous to the inverse deposition rate in experimental PVD. Films generated of 2000 molecules had an overall thickness of $\sim 70\sigma$ (examples shown in Figure S11A).

A flattened diagram of the model molecule can be seen in Figure 2A. Figure S11 shows examples of the films produced using this process for as deposited PVD films and after thermal transformation into the liquid quenched glass (LQG) states, as well as the radial distribution function of LQG of the two molecules, showing that the K=0 molecule has a larger density due to its ability to pack more efficiently. Using bulk MD simulations, the glass transition temperatures of the two model molecules were determined to be $T_{g,K=0}=0.70$ for the K=0 molecule and $T_{g,K=50}=1.24$ for the K=50 molecule, respectively. The SCL density, at T_g for each molecule was measured to be 1.08 for the K=0 molecule and 0.95 for the K=50 molecule, respectively. The LQG density and expansion coefficients of the SCL and LQG state each system are shown in table S1 of the SI.

The fictive temperature of as-deposited films were calculated by measuring the variations of the natural logarithm of the specific volume $(\ln(V))$ with temperature, in a manner analogous to the experimental procedure (Figures 2B). The T_f and the relative change in the specific volume $(\Delta \ln V = \ln V_{PVD} - \ln V_{LQG})$ upon transformation were calculated for films deposited at a range of T_{dep} for both K=0 and K=50 molecules as shown in Figure 6A&B, respectively. For each molecule, glasses deposited at lower temperatures than shown in these figures were unstable and had lower initial density than the corresponding LQG state (example shown in the inset of Figure 6). The shape of the molecules and their orientational order in the simulated PVD and LQG glasses, as well as the mean squared displacement (MSD) of molecules deposited under various

conditions and at various layers of the film were analyzed as detailed in the SI and Figures S12-14.

III. RESULTS

A. The Dependence of Thermal Properties on the Chemical Structure

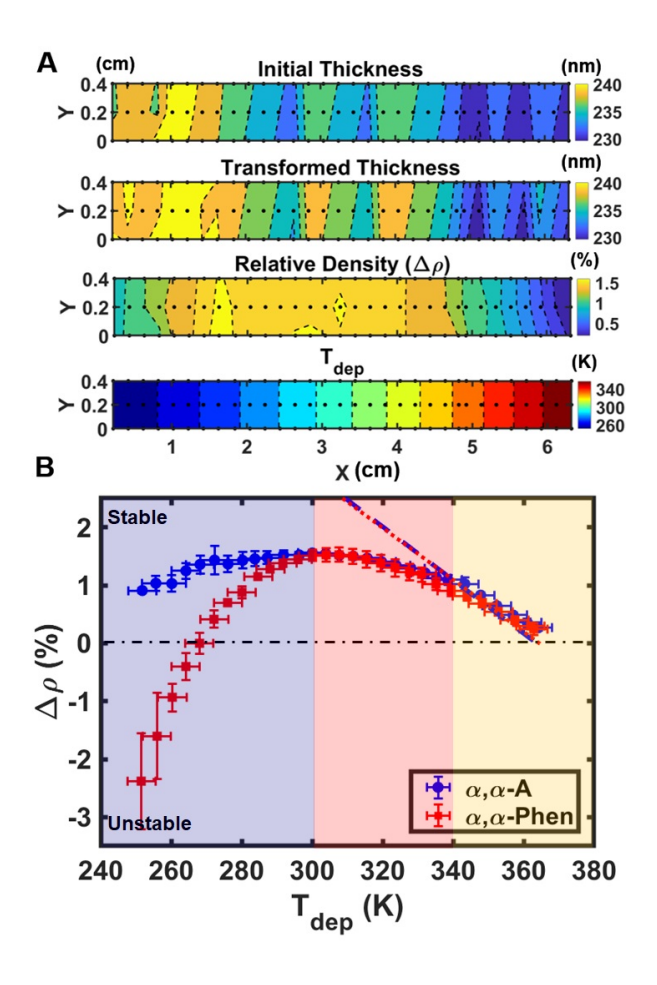


Figure 3. (A) From top to bottom, contour plots of as-deposited thickness, transformed (LQG) thickness, calculated $\Delta \rho$, and T_{dep} for a \sim 240 nm α , α -A T-grad sample. Black dots indicate the coordinates where SE data were obtained. (B) $\Delta \rho$ of \sim 240 nm PVD films of α , α -A (blue circles) and α , α -Phen (red squares) vs. T_{dep} . Dashed and dotted lines are the extrapolated SCL lines for α , α -A (blue) and α , α -Phen (red), respectively. The colors highlight three distinct deposition regions as detailed in the text.

a. Thermal stability of Vapor-Deposited Films. α, α -A and α, α -Phen have very similar liquid quenched glass (LQG) properties, with reasonably similar T_g and expansion coefficient values (Figure 1B and Table S1). However, they show markedly different behavior upon PVD as

shown in 3. For both molecules, within the error of T_{dep} determination, the relative density change $(\Delta\rho)$ follows the extrapolated SCL equilibrium lines at high deposition temperatures (340 $K < T_{dep} < T_g$, yellow highlighted region), producing stable glasses (SGs) with similar degrees of thermal stability. As T_{dep} is further decreased, $\Delta\rho$ deviates from the extrapolated SCL and reaches a maximum around $T_{dep} \sim 300$ K ($\sim 0.82T_g$, pink region) for both compounds. At low deposition temperatures ($T_{dep} < 300$ K, purple region), the properties of the two molecules deviate strongly. α , α -A films continue to produce stable glasses with $\Delta\rho_{-A} > 0$, over the entire T_{dep} range available in these experiments. In contrast, the stability in α , α -Phen films rapidly drops with decreasing T_{dep} . PVD films of this molecules become unstable below $T_{dep} < 264$ K forming glasses that are less dense than the LQG ($\Delta\rho_{-Phen} < 0$). We note that there are slight differences between the measured values of $\Delta\rho_{-A}$ in this study and those we reported previously²³. We attribute these differences to calibration issues for our previously reported T_{dep} values (more details in the SI and Figure S15). However, the overall the trends showing a broad range of T_{dep} where stable glasses are formed in α , α -A are similar in both studies.

B. Molecular Shape and Structural Anisotropy

a. Molecular Shape. Figure 2A shows the equilibrium shape and dimensions of α , α -A and α , α -Phen molecules obtained using DFT calculations (more details in the SI and Figure S10). At equilibrium, the dihedral angle of the A-diarylbenzene bond in α , α -A is $\sim 90^{\circ}$ and the molecule has roughly equal size in all three main directions (1.2 nm) meaning that the molecule is spherical. This value is consistent with the reported dimensions of α , α -A molecules in their crystalline form, as measured by X-ray diffraction²³. Given the high energy barrier (~ 20 Kcal/mol, ~ 33 KT) and for this dihedral rotation as well as its high angle at equilibrium, this molecule is expected to be rigid and mostly maintain its spherical shape with a small range of vibrations around its dihedral angle, particularly at low deposition temperatures. The equilibrium value for the Phen-diarylbenzene bond is $\sim 57^{\circ}$, giving the molecule a more flattened elliptical shape (1.4 nm along its long axis). With its lower energy barrier for rotation (~ 13 Kcal/mol, ~ 22 KT), the Phen-diarylbenzene bond can rotate almost freely in the SCL state. As such, this molecule will have more variations in its shape when vapor deposited closer to T_g . However, at low T_{dep} , where unstable glasses are formed, the molecule is likely very rigid and will assume its flattened equilibrium shape, with a small range of vibration around the Phen-diarylbenzene bond.

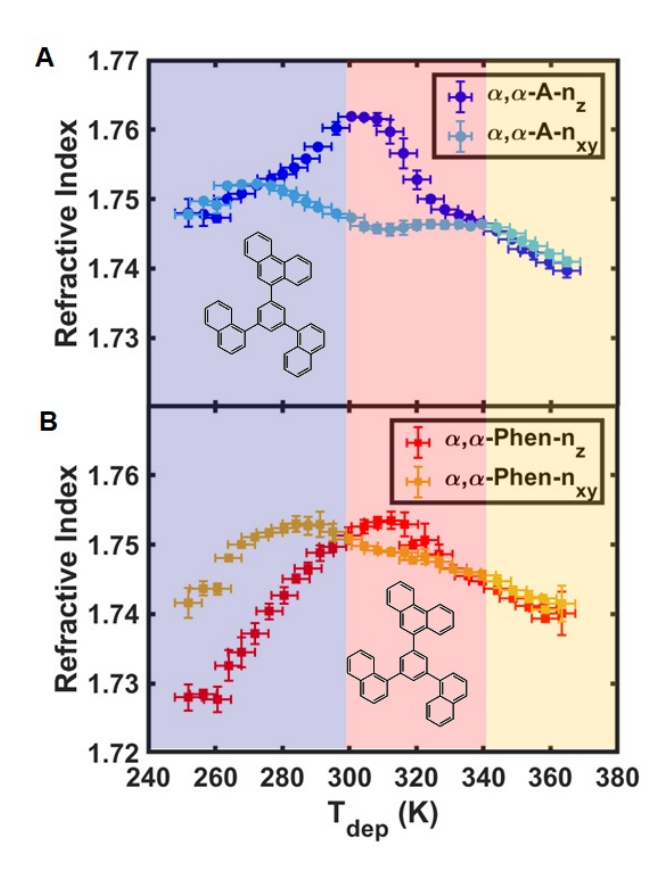


Figure 4. (A) Out-of-plane (n_z , dark-blue circles) and in-plane (n_{xy} , light-blue circles) indices of refraction of $\sim 1 \,\mu\text{m}$ PVD films of α , α -A vs. T_{dep} . (B) Out-of-plane (n_z , red squares) and in-plane (n_{xy} , orange squares) indices of refraction of $\sim 1 \,\mu\text{m}$ PVD films of α , α -Phen vs. T_{dep} . All indices were measured at λ = 632.8 nm. The color highlights correspond to the same regions as shown in Figure 3B.

b. Optical Birefringence and Orientational Order. Figure 4 shows the in-plane (n_{xy}) and out-of-plane (n_z) indices of refraction for $\sim 1\,\mu\mathrm{m}$ thick PVD films of α, α -A and α, α -Phen molecules (the measured values for \sim 240 nm films are slightly different and are shown in the SI figure S4). The average index of refraction of films made of both molecules correlate reasonably well with their at all T_{dep} values (Figure S5). This data provides an independent measure of density, without relying on transformation, and provides context for the overall non-monotonic trends observed n_z and n_{xy} of each molecule, which can be attributed to their density variations. The data in Figure 4 also shows strong differences in the temperature-dependence of n_{xy} and n_z , which reflects differences in their structural and orientational anisotropy. The color highlights in this figure correspond to the same regions as highlighted in Figure 3B. In the near-equilibrium region, where the density follows that of the extrapolated SCL equilibrium (340 K < T_{dep} < 368 K,

yellow region) stable glasses of both α , α -A and α , α -Phen are optically isotropic ($n_{xy} = n_z$), which is consistent with the notion that these glasses are reaching near-equilibrium thermal state during deposition.

As T_{dep} is decreased below 340 K (pink region), PVD glasses of both molecules show positive birefringence ($n_z > n_{xy}$). This effect is more pronounced in α , α -A SGs and is observed over a broader range of T_{dep} values. Given the rigid spherical shape of α , α -A molecules, the birefringence in these films can only be attributed to a spacing between their molecules in the z direction, as opposed to molecular orientation²³. We have previously measured the orientation order of the -A substituents in α , α -A SGs using polarized photoluminescence experiments²³, which provided direct evidence for isotropic molecular orientations in this range of deposition temperatures, despite their positive birefringence. Given their anisotropic shape, it is more difficult to separate layering and orientation in α , α -Phen films based only on their optical birefringence. However GI-WAXS experiments (Figure 5) confirm a similar but weaker layering structure in these films (more discussions in the next section), consistent with their relatively lower positive birefringence.

When T_{dep} is further reduced below ~ 300 K (passing the T_{dep} where maximum density is measured for both systems), α , α -A films gradually become more isotropic (purple region), indicating that their ability for molecular layering is reduced. In this regime, α , α -Phen films show negative birefringence ($n_z < n_{xy}$) indicative of the formation of in-plane molecular orientation 12,20 . This observation is consistent with the anisotroic shape of this molecule, which can promote in-plane molecular orientation at the surface layer during PVD. Both n_z and n_{xy} rapidly decrease in α , α -Phen films deposited below $T_{dep} < 270$ K, consistent with their reduced density.

c. Molecular Layering. While the positive birefringence in α , α -A films can be attributed to the molecule's tighter packing in the direction of deposition, it is not possible to separate the role of layering and orientational order in the measured birefringence of α , α -Phen films. To directly measure the degree of layering, GIWAXS experiments were carried out with $\sim 1 \, \mu \text{m}$ films of both molecules. Figures 5A&B show the 2D scattering patterns for α , α -A ($T_{dep} = 298 \, \text{K}$) and α , α -Phen ($T_{dep} = 289 \, \text{K}$) films. These are the deposition temperatures where the strongest structural anisotropy is observed in each system (data at other deposition temperatures are shown in Figures S7 and S8). Similar to previous studies in PVD glasses of other organic molecules 16,18,32 , both α , α -A and α , α -Phen glasses exhibit varying degrees of packing anisotropy, characterized by a difference in the integrated scattering intensity of the in-plane (q_{xy}) and out-of-plane (q_z) scattering directions in the scattering range of $q \sim 1.2 - 1.5 \, \text{Å}^{-1}$ (SI Figures S7 and S8), which

corresponds to the intramolecular structure of the molecules. In addition, a distinct anisotropic peak is observed in the q_z direction at $q \approx 0.59$ Å⁻¹ (Figures 5A&B as well as Figures S7 and S8). This value of q is roughly the same as the size of α , α -A or α , α -Phen molecules obtained using DFT calculations (~ 1.1 Å vs. 1.2-1.4 nm) and can thus be attributed to molecular layering (another indirect indication of tighter molecular packing in the direction of deposition) in these PVD glasses³².

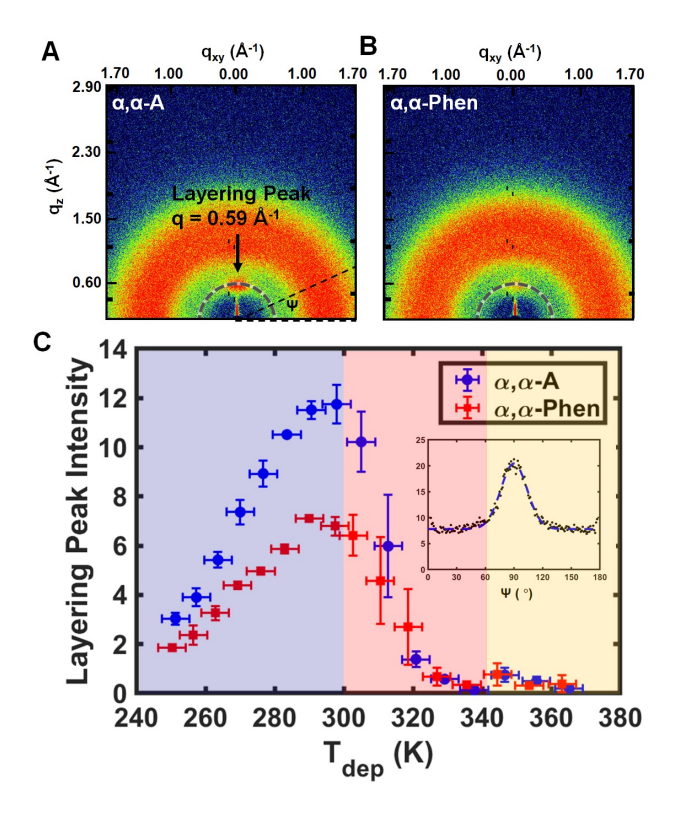


Figure 5. Two-dimensional GIWAXS scattering patterns for $\sim 1\,\mu\mathrm{m}$ thick PVD films of (A) α , α -A deposited T_{dep} = 298±4 K and (B) α , α -Phen deposited at T_{dep} = 289±4 K, respectively. These values correspond to the maximum layering peak intensity for each molecule. Both images have the same color scale, to highlight the stronger intensity of the peak in α , α -A films when compared with α , α -Phen. The variable, azimuthal integration angle Ψ and the location of the layering peak are indicated in (A). The dashed arc in (A) and (B) is the scattering region ($q = 0.59 - 0.69 \, \text{Å}^{-1}$) where the intensity of the layering peak is integrated. (C) Layering peak intensity vs. T_{dep} for α , α -A (blue circles) and α , α -Phen (red squares) PVD films. The inset shows the variations of peak intensity as a function of Ψ for data shown in (A). The peak intensity is measured as the amplitude of a Gaussian fit to this data (calculation details in the SI).

To quantify the strength of this layering peak, the accumulated scattering intensity in the radial

scattering range of $q_r = 0.56 - 0.62 \text{Å}^{-1}$ (dashed arc shown in Figure 5A) was plotted vs. the radial angle Ψ (example shown in the inset of Figure 5C). A Gaussian function was fitted to this data and its amplitude was designated as the scattering peak intensity. Figure 5C shows the calculated scattering peak intensity as a function of T_{dep} . Figure 5C shows that for glasses prepared with near-equilibrium structure ($T_{dep} > 340$ K, yellow region), there is no evidence of layering for either molecule, again indicating that isotropic, equilibrium structures were produced upon PVD. As T_{dep} is decreased below 340 K (pink region), the layering intensity grows, strongly correlating with the increased n_z in α , α -A. This strong correlation between n_z and layering peak intensity, in this otherwise spherical molecules, points out to the shared origin of the two phenomena. The layering peak intensity has a similar temperature-dependence in α , α -Phen, but is overall weaker (almost half the intensity at $T_{dep} = 298$ K), which is consistent with the molecule's smaller value of optical birefringence. It is notable that the density of both systems is similar in this region. This means that α , α -Phen molecules are forming packing structures that are closer to equilibrium. Our limited data for transformation kinetics of films deposited in this region ($T_{dep} = 298 \pm 4$ K, Figure S6) indicates that the kinetic stability of α , α -Phen is also improved compared to α , α -A despite similar density values, which is another indication of its improved stability. These variations merit further explorations in the future. The maximum layering intensity is measured at T_{dep} = 289±4 K for α , α -Phen, and at T_{dep} = 298±4 K for α , α -A. As the deposition temperature is further reduced (purple region), both systems show reduced layering peak intensity. However, it is notable that in both systems, some degree of layering is observed, indicating improved packing in the z direction, even in α , α -Phen glasses that are otherwise highly unstable. We note that in this molecule the index of refraction reflects a combination of packing anisotropy, which should result in increased n_z and orientational order, which should result in decreased n_z . These two effects cannot be separated, solely based on birefringence experiments.

C. The Structure and Stability of Simulated Molecules

In the simulated systems, where all three dihedral barriers are simultaneously varied, much larger differences are observed in the supercooled and liquid-quenched glass properties. While the overall shape of the model remains unchanged, the "K = 0" model, with its greater rotational freedom, can be thought of as a more flexible version of α , α -Phen and the "K = 50" model, with its more rigidly fixed side groups, can be thought of as more rigid version of α , α -A. These ex-

aggerated versions of the molecules allow us to produce stronger effects in the simulated systems. The K = 50 (more rigid molecule) has higher T_g , larger expansion coefficients, and lower density compared to the K = 0 model (Figures 2B, S11, and Table S1). This is because the rigid molecule has fewer configurations to adopt in order to relax and as such forms more frustrated packings.

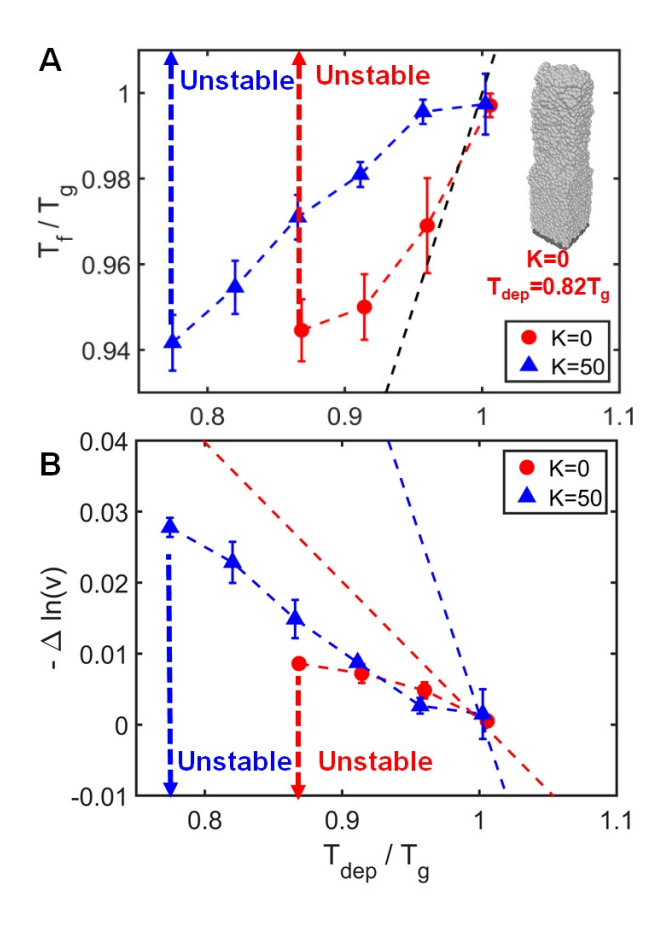


Figure 6. (A) Relative fictive temperature (T_f/T_g) vs. relative T_{dep}/T_g for simulated PVD glasses with K=0 (red) and K=50 (blue). The dashed black line indicates where $T_f=T_{\rm dep}$, representing the extrapolated equilibrium state. (B) The relative change in the log of specific volume ($\Delta \ln V$) for the same PVD films as in (A). The dashed lines show the corresponding extrapolated SCL values for the K=0 (red) and K=50 (blue) models. The red and blue arrows in both graphs indicate the direction of change in the corresponding values if the deposition is performed at a lower relative T_{dep} for each system. The inset of (A) shows an example of the packing of an unstable film of K=0 molecule deposited at $T_{dep}=0.82T_g$, which has a rough, low-density morphology.

The thermal stability of the simulated PVD glasses also show larger differences. Figure 6 shows the relative fictive temperatures (T_f/T_g) and the relative change in the specific volume (analogous

to the relative density change in experiments) for the K = 0 and K = 50 films deposited at a range of relative deposition temperatures (T_{dep}/T_g) . These values were calculated based on the plots of ln(V) as shown in Figure 2B. For the deposition range of $0.87T_g < T_{dep} < T_g$, PVD films of K = 0form glasses with lower T_f values (more stable) than those of the K = 50 model (Figure 6A). It is however notable that this difference in stability primarily arises from the differences in the SCL states of these molecules as can be seen in Figure 6B. The relative change in the specific volume of the PVD and LQG states (V_{PVD}/V_{LOG}) are similar between the two model molecules down to a deposition temperature of $\sim 0.87T_g$, while the extrapolated volume of the SCL state (dashed lines in Figure 6B) vary significantly. This is consistent with the experimental data at high T_{dep} , where the density change as measured in the glass state is similar between the two molecules. However, given their drastically different SCL expansion coefficients, the K = 50 films are farther from their corresponding equilibrium states (have higher T_f) at the same T_{dep} . For the experimental counterparts, the expansion coefficients of the SCL α , α -Phen is only slightly lower than that of α , α -A ($\alpha_{SCL,-Phen} = (5.5 \pm 0.05) \times 10^{-4} \text{ K}^{-1} \text{ vs. } \alpha_{SCL,-A} = (5.6 \pm 0.1) \times 10^{-4} \text{ K}^{-1} \text{ as shown}$ in Table S1), which makes such differences in the relative stability in the high T_{dep} region more negligible. However, it is notable that α , α -Phen films have improved kinetic stability (resistance to transformation, Figure S6) compared to α , α -A films deposited at the same temperature, which indicates while density changes are not significant, their effective "age" is different, consistent with the simulations.

As shown in Figure 6, The K=0 molecules reach their maximum stability under the deposition conditions used here at $0.87T_g$, with a minimum $T_f\approx 0.94T_g$. When deposition is performed below this temperature, the K=0 molecules have low surface mobility and lose their ability to fully wet the glass during vapor deposition (example shown in the inset). As such, they form unstable glasses upon PVD with T_f and density values that exceed the limits shown in Figure 6, indicated by the dashed red arrows. Conversely, the K=50 models continue to form stable glasses down to a deposition temperature of $T_{dep}=0.77T_g$ ($T_f\approx 0.94T_g$, matching the lowest value of the K=0 model at $T_{dep}=0.87T_g$), before losing their ability to form stable glasses (indicated by dashed blue arrows). This is analogous to α , α -A molecule showing a larger window of stability compared to α , α -Phen upon vapor deposition at low temperatures (Figure 3B).

Simulated models also show variations in molecular shape and packing anisotropy that qualitatively mimic some but not all of the features observed in experiments. The average asphericity of the K=0 and K=50 model molecules are shown in Figure S12A (detailed calculations in

the SI). Both molecules are found to take a non-spherical shape, independent of the deposition temperature, distance from the free surface, or the glass state (PVD vs. LQG). However, on average the K=0 model shows more flattened shapes (larger asphericity) than the K=50 model, consistent with the experimental observations. We note that the dramatically large angle of the dihedral bond in the experimental α , α -A molecule is due to the steric hindrances caused by the interactions between the hydrogen atoms on the anthracene moiety at positions 2 and 6 and the hydrogen atoms on the central benzene moiety, which forces the anthracene substituent to bend in order to go through the transition state⁶¹ as shown in Figures S10E-S10G. This interaction is not present in the coarse-grained model molecules, making them more likely to take non-spherical shapes even in the K=50 model. As such, it is not surprising that α , α -A molecule is more rigid in shape than its simulated counterpart, despite having only one very restricted dihedral rotation.

IV. DISCUSSIONS

A. The Role of Molecular Shape and Dihedral Energy Barriers in Stability

In α , α -Phen, the deposition region where a strong in-plane molecular orientation is observed (T_{dep} < 300 K, purple region in Figure 4B) coincides with the same region where thermal stability is rapidly diminished as seen in Figure 3B. It is thus tempting to assume that molecular orientation contributes to this dramatic reduction in stability. However, this picture breaks down in the simulated systems. In simulations, a small degree of in-plane orientation is observed in both K=0 and K=50 PVD films (Figure S12B), which becomes stronger as the deposition temperature is decreased. However, there are no significant differences in the temperature-dependence of the orientation order of the two model molecules, despite their different degrees of stability as measured by T_f . It is important to note that both molecules have asphericity values that are not dramatically different (Figure S12A) and remain constant as a function of T_{dep}/T_g and they both have similar relative specific volume as the same relative T_{dep}/T_g (Figure 6B), thus it is not surprising that both systems form anisotropic structures upon PVD that are not significantly different.

However, flexibility of the bond angles plays a stronger role in the observed stability trends in both experiments and simulations, across the entire window of the deposition temperatures. The simulated systems have a larger difference in their barriers for dihedral rotations, and show a larger contrast in their propensity to find low-energy states in their energy landscape. Even at the

same deposition temperatures and the same relative density (Figure 6B), the K = 50 molecules are farther from their corresponding equilibrium states, than the K=0 molecules. The origin of these differences in stability lies in the corresponding structure of the SCL equilibrium state, as opposed to the PVD glass. While the inter-molecular interactions are conserved, the added flexibility in these systems can dramatically affect the energy landscape by providing more entropic degrees of freedom. The ability of the flexible molecules (K = 0) to internally relax through dihedral rotations (larger configurational entropy) allows them to pack more efficiently and more closely, resulting in higher density of the equilibrium states (dashed lines in Figure 6B) at the same relative temperature below T_g . The K = 50 molecules have more frustrated packings and fall out of equilibrium at a higher T_g value, where they can no longer relax. As such, liquid-quenched glasses produced by this molecule have lower density and larger anharmonicity (expansion coefficient, as shown in Table S1) than the K=0 molecules at the same temperature relative to T_g . These differences in the expansion coefficient of the SCL state are more subtle in the experimental systems (Table S1), but nevertheless, our limited data indicates that they show improved kinetic stability at high T_{dep} (Figure S6) and lose their ability to form SGs faster at low T_{dep} , analogous to their simulated counterparts (Figures 3B).

B. Surface Mobility, Mobility Anisotropy, and Mobility Gradients

It is counter intuitive that the more flexible molecules, which are able to sample more configurations at the free surface, cannot form better stable glasses at all deposition temperatures as seen in both experiments (Figure 3B) and simulations (Figure 6). To understand this phenomenon, it is critical to consider how surface mobility and mobility gradients are affected by molecular flexibility. MD simulations provide a direct path to measure mobility as a function of depth from the free surface in both LQG and PVD states. The mobility of the model molecules were measured by calculating the mean squared displacement (MSD) of particles, evaluated at a particular lag time of $t = 9 \times 10^4 \tau$, where τ is the standard LJ time unit. This lag time represents the τ_{α} for a particle of either model molecule at its corresponding T_g . This standard lag time was used to compare the inplane ($< r^2 >_{xy}$) and out-of-plane ($< r^2 >_z$) mobility in 2σ -thick layers at various depths in PVD and LQG films, at various temperatures, and under different deposition conditions (more details in SI and Figures S13 and S14). Figure 7 shows the gradients of in-plane and out-of-plane mobility, in LQG films of both K = 0 and K = 50 molecules, as well as the corresponding data for somewhat

stable ($T_f = 0.97T_g$) and most stable ($T_f = 0.94T_g$) glasses of each model molecule, all measured at $0.82T_g$. The high and low T_f glasses were deposited at $T_{dep} = 0.97T_g$ and $T_{dep} = 0.87T_g$ for the K = 0, and $T_{dep} = 0.87T_g$ and $T_{dep} = 0.77T_g$ for the K = 50 molecules, respectively. In all six films and in both directions, the mobility is enhanced at the free surface compared to the film's center.

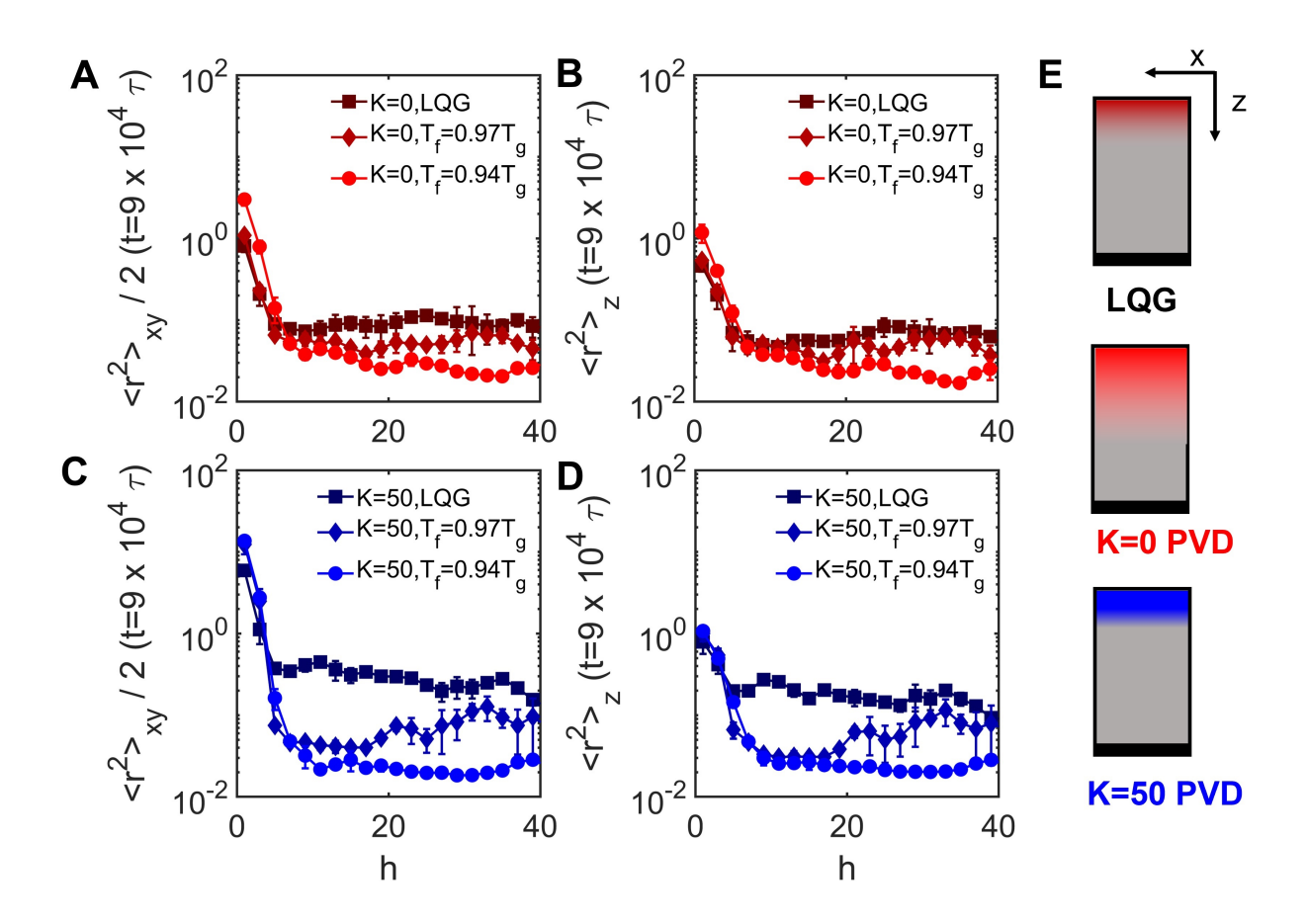


Figure 7. (A) Lateral ($\langle r^2 \rangle_{xy}$) mobility and (B) vertical ($\langle r^2 \rangle_z$) mobility in LQG (dark red squares), PVD with $T_f = 0.97T_g$ (red diamonds), and PVD with $T_f = 0.94T_g$ (light red circles) films of K = 0 molecule measured in 2σ -thick layers vs. distance from the free surface, h. (C)-(D) The corresponding mobility values for K = 50 films. All MSD values were measured at a relative temperature of $0.82T_g$ and a lag time of $t = 9 \times 10^4 \tau$. (E) Schematic demonstration of the shape of the mobility gradient in LQG films vs. PVD films of each model. Surface mobility falls more rapidly (sharper gradient) from the free surface in K = 50 PVD films compared to K = 0 films with the same relative T_f/T_g .

The gradients of mobility however, strongly vary in the in-plane (lateral, xy) and out-of-plane (vertical, z) directions for both model molecules, indicating that the surface mobility is anisotropic and is influenced by the bulk glass structure. Evidence for such mobility anisotropy has long been

observed in simulated glass-forming polymers⁶⁵ and metallic glass systems⁶⁶. Notably, for the most stable PVD glasses ($T_f = 0.94T_g$) of both molecules, the free surface shows noticeably faster mobility in the lateral (xy) direction compared to the LQG at the same temperature, as shown in Figure 7A&C. Given that the film center also has slower mobility (due to improved stability), this excess enhanced surface mobility translates into stronger mobility gradients (larger surface to bulk ratio of $< r^2 >_{xy}$) as well as a larger thickness over which the dynamics are enhanced compared to the film's center (larger length scale of mobility gradients, as schematically shown in Figure 7E). Interestingly, unlike the K=0 molecule, the mobility at the free surface in the vertical (z) direction is similar in both PVD and LQG films for the K=50 model. However, the K=50 PVD system does show an enhancement in lateral (xy) surface mobility, similar to the K=0 model.

Nevertheless, the length scale of the mobility gradients in this direction still grows with decreasing T_f (more prominently seen in the K = 50 model), as the film center still has slower dynamics. In both LQG systems, the mobility becomes bulk-like and relatively isotropic at a distance $\sim 6\sigma$ from the free surface of the film (Figure S14 C&F). In contrast, in the most stable K = 0 PVD film $(T_f = 0.94T_g)$, the distance to reach bulk-like mobility is up to $16 - 18\sigma$, in both lateral and vertical directions (Figure 7 A&B). For the most stable K = 50 PVD film ($T_f = 0.94T_g$), this distance is $12-14\sigma$ in-plane and $10-12\sigma$ out-of-plane (Figure 7C&D). Overall, this behavior results in a sharper gradient in PVD films compared to the LQG as schematically shown in Figure 7E. For example, the ratio of the surface to bulk mobility, in the lateral xy direction, is ~ 8 for the K=0LQG film while it increases to \sim 115 for the K=0 PVD film. Lastly, even at the same relative T_f , the K = 50 model molecules show stronger enhancement of in-plane mobility at their free surface, and slower dynamics relative to LQG at their center, generating even sharper gradients than the K=0 films. For the K=50 films, the ratio of the surface to bulk mobility in the xy direction is \sim 25 for the LQG and \sim 705 for the PVD films, respectively. These rather large gradients are partially due to the fact that the film center is less mobile for the LQG of K = 50 than K = 0 at the same relative temperature (indicating higher fragility in these films).

To better understand the details of this phenomenon and how it affects stability upon PVD, it is informative to evaluate the surface mobility and its anisotropy (quantified as the ratio of the in-plane and out-of-plane mobility ($\langle r^2 \rangle_{xy} / \langle r^2 \rangle_z$)) over a broad range of measurement temperatures. For each model molecule, the mobility of the LQG films were measured in each direction, at temperatures below T_g , and for 2σ -thick layers at the free surface and the film center (depth of 30σ). The resulting mobility anisotropy values are shown in Figure 8 along with the

corresponding data for the stable glass PVD films, examined at two different temperatures (same stability conditions as the data in Figure 7). Not surprisingly, the mobility in both directions and at both the free surface and the film center decreases with decreasing temperature (Figure S13). However, the temperature-dependence of mobility is different in the two directions and between the two molecules. As shown in Figure 8A a non-monotonic trend emerges in the mobility anisotropy of the free surface as temperature is decreased, while as expected, the mobility remains isotropic at the film center (8B), where there is no distinctions in the barriers for relaxations in each direction.

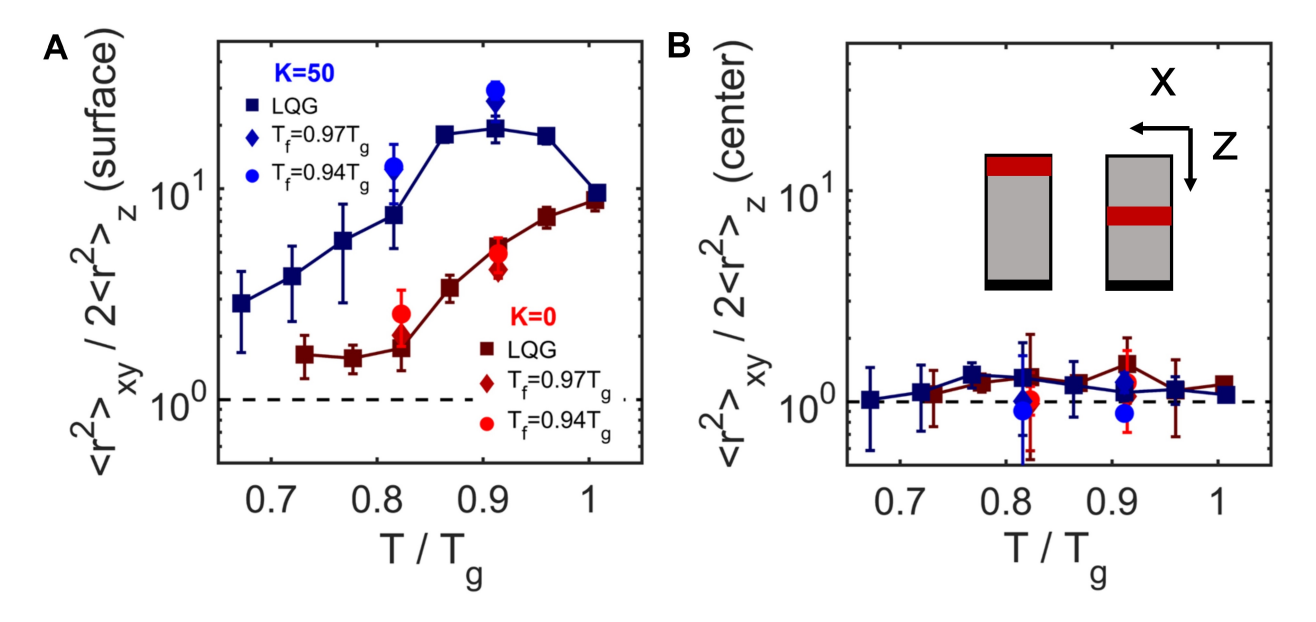


Figure 8. (A) Mobility ansiotropy at the free surface, measured as the ratio of the in-plane ($\langle r^2 \rangle_{xy}$) and out-of-plane ($\langle r^2 \rangle_z$) mean squared displacement at a lag time of $t=9\times 10^4\tau$, for particles in LQG films (dark squares connected by solid lines) and two different PVD films, $T_f=0.97T_g$ (diamonds) and $T_f=0.94T_g$ (light circles), vs. relative measurement temperature for K=0 (red) and K=50 (blue) model molecules. The mobility anisotropy is measured in a layer 2σ thick at the free surface. (B) The corresponding values measured at a layer 2σ thick buried 30σ from the free surface (film center). The inset schematically shows the location of the surface and center layers, as well as the coordinates of measurements.

At the free surface, the particles have greater ability to diffuse laterally (xy direction), where their motion is not strongly affected by the potential induced by the layers below. This is consistent with experimental observations of enhanced surface diffusion^{41,45,47}. The degree to which the surface molecules have excess in-plane mobility, decreases with decreasing temperature, indicating

that the free surface also falls out of equilibrium at some point below bulk T_g and is also consistent with previous experiments and simulations in thin-films where T_g is reduced^{44,65,67}. However, the temperature dependence of mobility in the two directions are different, resulting in mobility anisotropy. For the K=0 molecule, the maximum mobility anisotropy is seen at T_g , starting at a value around 10. As the temperature is decreased from there, the mobility anisotropy steadily decreases before hitting a plateau around $0.82T_g$. This is close to the deposition temperature below which PVD films become completely unstable (Figure 6). Looking at the corresponding mobility gradients (Figure 7), it appears that the motion of K=0 model molecules couple more strongly to their corresponding bulk values at this temperature compared to the K=50 model molecules, resulting in a loss of excess mobility, which translates to decreased mobility anisotropy and thus ability to form stable glasses upon vapor deposition.

For the K = 50 molecules, the ratio of mobility in the lateral and vertical directions also starts at around 10 at T_g . However, this ratio grows and the mobility anisotropy reaches a peak value of 20 at $0.91T_g$. At this point, the surface mobility is significantly enhanced compared to the bulk mobility in the lateral direction, which impedes the molecule's ability to form a stable glass due to fast motion that is strongly decoupled from the dynamics of the layers below. This is presumably due to reduced packing efficiency of the K = 50 molecules, which allows them to freely move at the surface, analogous to fast and invariant surface diffusion previously observed in an experimental PVD system with rapid surface diffusion⁴⁷. As the temperature is further decreased, the anisotropy ratio decreases, allowing the formation of more stable glasses when the dynamics are better coupled to the rest of the glass. However, the plateau in anisotropy ratio is not reached until much lower temperatures. As previously shown in Figure 6, compared to the K=0model molecule, the K = 50 model molecules produce stable glasses over a broader range of deposition temperatures, but do also become unstable at a point where this ratio becomes roughly equal to \sim 4 (compared to \sim 2 for K=0 films). At both unstable temperature cutoffs, the absolute in-plane surface mobility ($< r^2>_{xy}/2$) at this characteristic timescale dips below $\sim 2\sigma^2$ (as can be seen in Figure S13D), preventing full equilibration upon deposition.

During PVD, both surface mobility and mobility anisotropy are slightly different than that of the LQG surface. However, these variations do significantly change the broader picture of how flexibility can affect stable glass formation. The K = 0 films have consistently smaller mobility anisotropy at the free surface, and their excess surface mobility of their PVD films when compared to LQG films are more in tandem in the lateral and vertical directions (Figure 7A&B). The

K=50 films show much larger mobility anisotropy at the free surface of both LQG and PVD films, indicating that surface molecules have a difficult time penetrating into the film, and dynamically coupling to the bulk energy landscape. While PVD films of this model show enhanced lateral mobility, they show no improvement compared to LQG films in the vertical direction. Additionally, the thicknesses of the mobile regions are shorter for the K=50 films in general. The relative lack of configurational entropy for the more rigid K=50 molecules likely results in less efficient packings upon PVD, which cannot readily age into stable states. This seems to drive the mobile/bulk region dichotomy to a greater degree in this system, resulting in thinner mobile regions with sharper transitions. These observations indicate that while the absolute mobility of the molecules at the free surface are important in allowing them to form stable glasses, the details through which the surface mobility couples with the mobility at the film's center (mobility gradients) and how it slows due to inter- and intra-molecular relaxations can play a significant and non-trivial role in the degree of stability of vapor-deposited glasses. The mobility anisotropy appears to be as important as the mobility itself in governing the properties of PVD glasses.

While it is significantly more difficult to measure the mobility gradients and their anisotropy in experiments, our data provides convincing evidence that a single change in the barriers for the dihedral rotation can have a profound impact on the surface mobility profile as indirectly measured through the stability of PVD films. The first indirect evidence of variation in surface relaxation times can be provided by measuring the dewetting of thin PVD glass films. We have previously demonstrated that enhanced surface mobility can result in enhanced dewetting rates in thin molecular glass films^{42,49,67}. While a comprehensive thin film dewetting study is outside the scope of this study, we can compare the as-deposited morphology and its evolution in thin films of both molecules with the same thickness. Figures 9A&C show that when deposited at T_g , asdeposited α, α -A thin films (\sim 24 nm) are smoother and have a smaller dewetted area (exposed substrate) than α , α -Phen films with the same thickness. When the two partially dewetted films are annealed at a temperature just below T_g for a set amount of time (90 min at 0.92 T_g , Figures 9B&D) the morphology of the α , α -A evolves very slowly, while α , α -Phen thin films show significant coarsening and dewetting. The results here suggest that, the average mobility of the 24 nm α , α -Phen film is faster than that of α , α -A at 0.92 T_g . This is within the deposition temperature range where near-equilibrium structures are formed upon PVD (Figure 3B). Considering our previous report on 10 nm films of α , α -A, which also exhibited substantial dewetting⁴⁹, and the rough morphology of the as-deposited 24 nm α , α -A films indicating some dewetting occurs during

deposition at T_g , we can conclude that enhanced surface relaxations still exist at the α , α -A surface. However, the length scale of the mobile surface layer is likely smaller in α , α -A than that of α , α -Phen⁴⁴. It is important to note that thin film dewetting experiments cannot precisely measure the length scale on the surface of PVD glasses, which can be different in magnitude and their anisotropy as shown in Figure 8. Future experimental methods need to be developed for direct observation of mobility on the stable glass film surfaces to resolve these details.

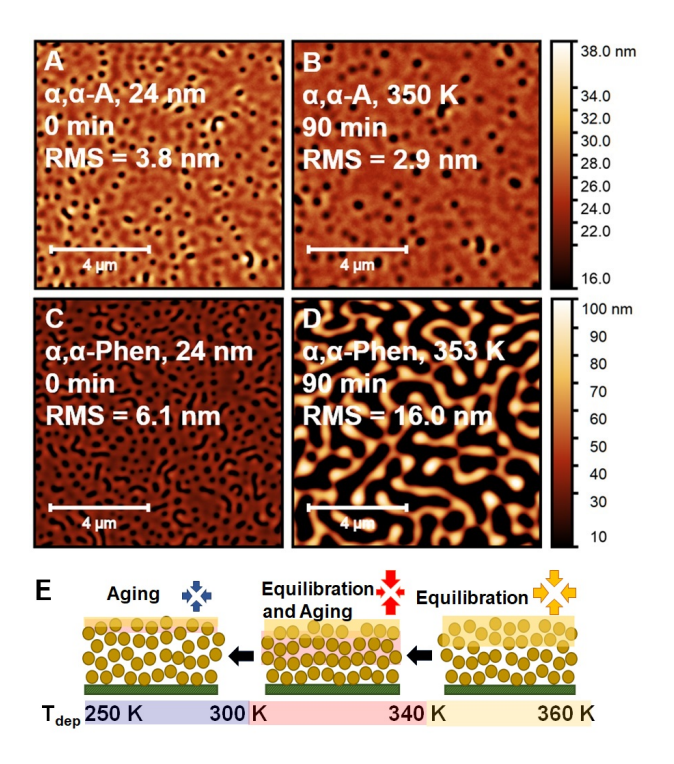


Figure 9. (A) AFM measurements of the initial morphology of a 24 nm film of α , α -A deposited at $T_{g,A}=364$ K. (B) The film morphology in the same area after 90 min of isothermal annealing at 350 K (0.92 $T_{g,A}$). (C) The initial morphology of a 24 nm film of α , α -Phen deposited at $T_{g,Phen}=366$ K. (D) The film morphology in the same area after 90 min of isothermal annealing at 353 K (0.92 $T_{g,Phen}$). Grain wise mean square roughness (RMS) is labeled in each figure. (E) Schematic diagrams for the structure of α , α -A in the three deposition regions. As the deposition temperature is decreased, the thickness of the equilibrium mobile region (highlighted in yellow) decreases, as some portion of it falls out of equilibrium resulting in a region with accelerated aging (highlighted in pink) which contributes to layering, as schematically shown by tighter packing in the direction of deposition. As the deposition temperature is further decreased, the thickness of both equilibrium and aging layers further decrease, decreasing both stability and layering, gradually forming more isotropic, but less stable structures.

C. Understanding the Evolution of Surface Mobility Through the Evolution of Structural Anisotropy.

While as discussed in section IV A, While the molecular shape and structural anisotropy do not appear to directly affect stability (Figure S12), the emergence of layering and orientational order can be used as proxy to understand the nature of surface mobility and its mobility anisotripy. Both layering and molecular orientation have their origins at the free surface region, where the system is exploring its pathway towards equilibrium and the equilibrium structure of the surface layer can be anisotropic ¹⁰. As such, understanding this interplay between layering and orientation, can inform us about the mobility profiles at the free surface. Here, we show how the growth and decay of the layering peak can be used as a proxy for the presence of surface-mediated aging (SMA), where some portion the surface region is out of equilibrium but has an accelerated rate of aging compared to the bulk, while the emergence of in-plane orientation can be used as a proxy for the reduced thickness of the equilibrium mobile layer, where surface-mediated equilibration (SME) can occur on the time scale of deposition. The interplay between these two regions can indirectly elucidate the dynamical gradients of the mobile surface layer.

Molecular layering, typically observed in GIWAXS experiments at a length scale corresponding to the molecule's size, has been ubiquitously seen in vapor-deposited glasses 18,31,32,35. The appearance of this structure cannot be directly attributed to a specific preferred orientation of molecules. For example, layering is observed in spherical molecules such as α , α -A²³ and Alq3³² that cannot orient along a specific direction. In addition, as shown in Figure 5C the temperature-dependence of layering is similar in α , α -A and α , α -Phen molecules, even in regions where α , α -Phen has in-plane orientational order (T_{dep} < 300 K, purple region). However, in non-spherical molecules, the decay of this peak at low temperatures coincides with the range of T_{dep} where the in-plane orientational anisotropy grows, as measured through the birefringence of the index of refraction. This can be seen in comparison between Figures 4B and 5C for α , α -Phen (purple region) as well as in previous experiments in indomethacin molecules⁶⁸. It is also important to note that birefringence experiments, performed in the transparent region of the spectrum, are not able to separate the effect of layering (changes in the radial distribution function in a specific direction) and molecular orientation (preferred orientation of an induced dipole of the molecule), as the two variables have a linear effect on the dielectric permittivity of the material²³. Thus, it is not possible to readily separate the role of layering and orientation in non-spherical molecules, or understand the origin

of this correlation. The unique molecular systems used in this study do however, provide an opportunity for such separation. Both molecules have similar polarizability, as is evident by their similar average index of refraction values close to T_g in thick films (Figure S5C). They also have similar intermolecular interactions, as they are isomeric molecules. Their only difference arises from their different barriers for rotations around a single bond, resulting in differences in their equilibrium shape as well as their flexibility.

Given its demonstrated lack of orientational order²³ and its spherical shape, it is easier to first focus on the structural details of α , α -A and make comparisons with α , α -Phen when necessary. Vapor-deposition of α , α -A close to T_g (yellow highlighted regions in Figures 3-5) produces glasses that are isotropic with no evidence of layering during deposition, with densities close to that of their extrapolated equilibrium structure. By all measures, these glasses appear to have enough mobility, in a thick enough region of the free surface (schematically shown in Figure 9E), to optimize their configuration in both lateral and vertical directions and reach near-equilibrium states before being buried deeper into the film. While the surface mobility of α , α -A is likely slower than that of α , α -Phen in this regime (Figure 9), the surface mobility is large enough for both molecules to reach equilibrium at the chosen deposition rate of this study. In addition, the thickness of this layer is at least a few times the size of the molecule, to allow full reorientation and equilibration of α , α -Phen molecules, well below the immediate free surface^{35,39}. This is a regime where surface-mediated equilibration (SMA) is the dominant process for forming stable glasses, as had been previously simulations⁶⁹. We note that this near-equilibrium deposition condition is not met in any of our simulated PVD films, as the timescales of simulations are not long enough at any T_{dep} , and T_f is always measured to be larger than T_{dep} , but nevertheless, some reorientation is observed when a highly anisotropic molecule was studied³⁹.

In the intermediate range of deposition temperatures (300 K $< T_{dep} <$ 340 K, pink region) the density of as deposited α , α -A molecules deviate from the extrapolated equilibrium conditions, with the differences increasing as T_{dep} is decreased, reaching a maximum density at $T_{dep} \sim$ 300 K. In the spherically-shaped α , α -A molecule, both n_z (Figure 5A) and the layering peak intensity (Figure 9C) grow simultaneously, correlating strongly with the increased density²³, while n_{xy} remains relatively constant (Figure 5A). One can rationalize this observation by hypothesizing that in this temperature range a portion of the mobile layer falls out of equilibrium at some distance not far from the free surface (schematically shown in Figure9E), but the molecules still have enough mobility to age at a rate faster than the bulk physical aging rate. Surface-mediated accelerated ag-

ing (SMA), under the constraint of the rigid stable glass layer underneath, can produce anisotropic packing. As the mobile layer ages towards equilibrium, molecules can decrease their packing distance in the z direction (increasing n_z), while the packing in the xy plane is constrained, resulting in relatively constant n_{xy} values for α , α -A. The resulting increased density in these kinetically trapped structures, are thus mostly due to tighter vertical packing of the molecules as opposed to finding isotropic equilibrium states. It is notable that with its more flexible structure, α , α -Phen has similar density values as α , α -Phen in this region, while also showing a smaller extent of molecular layering as seen in Figure 5C. In addition, the value of n_{xy} for α , α -Phen does not reach a plateau in this region (pink highlighted region in Figure 4B). Combined, these observations indicate that the thickness of the "equilibrium" liquid layer of this molecule is larger, with a more limited range where it goes through accelerated aging, consistent with its increased configurational entropy. These experimental observations are consistent with the simulations that show a smaller mobility anisotropy in the more flexible K = 0 model at high deposition temperatures. Accelerated aging of the surface region has been directly observed in recent in situ experiments of the dielectric constant of 2-methyltetrahydrofuran molecules around $0.82T_g^{37}$, which corresponds to the same relative T_{dep} as α, α -A and α, α -Phen deposited around 300 K. As the deposition temperature is further reduced (250 K $< T_{dep} < 300$ K, purple region) the layering peak intensity for α , α -A decreases slowly, but does not reach zero in the experimental range accessible to this study. This indicates that not only has the surface layer is mostly out of equilibrium with limited lateral mobility, preventing the formation of stable glasses, but the effective aging rate and/or the thickness of the SMA region is also reduced, as schematically shown in Figure 9E.

The non-monotonic temperature-dependence of the SMA process is analogous to the non-monotonic temperature-dependence of physical aging in bulk systems, where an interplay between slowing relaxation times and increasing depth of the energy landscape influence the maximum aging rate. However, here the effective aging time is dictated by the deposition rate. As such, we hypothesize that if the molecular layering is indeed an indication of SMA, a strong dependence should exist between the location and intensity of the layering peak intensity and the deposition rate. This means that faster deposition rates should provide a narrower window of layering and weaker layering peak intensities. Indeed previous experiments in indomethacin have shown evidence for such behavior 16 . The strong correlation between the density and the layering peak intensity as well as n_z , in the absence of molecular orientation also indicates that in this region, the stable glass formation itself is through an out of equilibrium accelerated aging at the free surface,

with aging rates that are significantly faster than those in bulk glasses. This hypothesis provides a self-consistent picture of how stable glasses are formed through an interplay between surface-mediated equlibration (SME) and surface-mediated accelerated aging (SMA) in the near surface region without the need for any preferred molecular orientation. In addition, the temperature where the layering peak is observed at a given deposition rate, can be used as a proxy for the effective $T_g(s)$ of the mobile surface at the corresponding cooling rate. As such GIWAXS experiments of the deposition rate- and deposition temperature-dependence of the molecular layering, can reduce the need for direct measurements of surface mobility and surface T_g , which are typically much more complicated to perform.

Based on the limited observations in our simulated data (Figure 7), we expect significantly enhanced surface aging rate in stable glasses compared to the surface of LQG. This can explain why significant stability is achieved upon PVD with moderate enhancement of surface mobility. If so, one would expect some degree of thickness dependence in the intensity of the layering peak, as initially the deposition takes place on a glass that does not yet have this excess enhanced mobility. As a more stable glass is formed in the film center, the effective surface mobility is faster and the gradient expands over a broader range, thus allowing an effectively faster SMA rate, resulting in higher intensity of the layering peak. Indeed GIWAXS experiments performed on α , α -A films of various thicknesses (Figure S9) show a growth of the peak intensity with increasing film thickness, extending to films as thick as 1300 nm. This observation merits further in-depth investigation as it can elucidate the role of film thickness in the SMA process and provide a proxy to estimate the length scales of the accelerated aging region, which are critical in the glass stability in the kinetically trapped region. We caution that the thin film mobility profile itself may also be different as a function of the film thickness⁵⁹. Future experiments need to be carefully designed to rule out such effects.

The preferred molecular orientation that emerges in α , α -Phen films deposited below 300 K (purple region in Figure 4B) indicates that the thickness of the equilibrium mobile region for α , α -Phen molecules is also decreased to around or below one-molecular layer, forcing the molecules to adopt configurations that correspond to the immediate free surface of the liquid. It is also possible that this orientation is adopted near the interface between the mobile layer and the out-of-equilibrium layer below as has been recently demonstrated³⁴. Regardless, the interface at which the glass is falling out of equilibrium is inducing the orientation order in these molecules. As such, it is not surprising that the emergence of this layer coincides with the region where the accelerated

aging rate is slowing down, preventing the molecules from further reorientation and relaxation as they continue to be buried into the glass film. The comparison between α , α -Phen and α , α -A molecules in this region shows that while both stability and molecular orientations are induced by the mobility gradients of the free surface, the two phenomena do not have to be correlated. In non-isotropic molecules, isotropic packing provides strong evidence for achieving equilibrium structures through SME, as it is also evident by the deposition rate-temperature superposition of anisotropy³⁵. However, the existence of in-plane anisotropy does not always mean that liquid-crystalline order is produced, but that the glass does not have enough surface mobility to rearrange below its immediate free surface. In addition, a positive birefringence does not necessarily mean out-of-plane orientation, as accelerated aging can also contribute to a positive value of birefringence. As such, careful control experiments are necessary to separate the role of each variable in the measured positive birefringence.

D. The Important Role of Intramolecular Relaxations in Glass Properties.

Perhaps the most important aspect of the data presented in this study is not in the exact details of the produced structures but the profound impact of variations of the intramolecular degrees of freedom (molecular level flexibility) on the supercooled liquid and the liquid-quenched glass properties. It is often convenient, particularly in MD simulations and simple models of glass transition, to vary inter-molecular interactions as a route to change the configurational entropy of the glass. However, these approaches can be limiting in the number of ways the configurational entropy can be modified and in their direct relevance to the experimental data in complex molecules. Our data, provides an alternative pathway to modify glass properties. Simulations show that T_g , expansion coefficients, equilibrium density, and stability in both LQG and PVD states can be modified through variations in intramolecular degrees of freedom. Our experimental data show that changing the barrier of rotation for even a single bond can be enough to produce glasses with significantly different structures, kinetic, and thermal stability upon PVD. This strategy can be adopted as a design principle to produce PVD glasses with independently varying degrees of stability and structural anisotropy. It can also be used as a new approach to separate the entropic (through molecular flexibility) and enthalpic (through inter-molecular interactions) contributions to the properties of glass-forming materials.

V. SUMMARY AND CONCLUSION

In this work, we design structurally similar isomeric molecules with subtle differences in their rotational barrier and thus molecular shape (spherical vs. flattened ellipsoid), in both experiments and coarse-grained molecular dynamics (MD) simulations, to gain insight into the interplay between molecular level structure and flexibility and the properties of vapor-deposited stable glasses. We demonstrate that molecules with more flexible bond rotations have enhanced surface mobility and can pack more efficiently when deposited close to the glass transition temperature T_g , where surface-mediated equilibration (SME) is the dominant process. However, the more rigid molecules are able to maintain enhanced surface mobility and access accelerated surface aging rates over a broader range of deposition temperatures, due to their inefficient coupling to the bulk, thus forming stable glasses at much lower temperatures than their flexible counterparts.

Through experimental measurements of molecular layering, optical birefringence, and MD simulations, we demonstrate that the flexibility of molecules plays a strong role in the enhancement of mobility at the free surface as well as the ability of the molecule to dynamically couple with the layers directly below, which in turn limits the range of temperatures over which the dynamics remain enhanced and at equilibrium. Furthermore, we demonstrate the the surface mobility, mobility gradients, and mobility anisotropy (the difference between the in-plane and out-of-plane relaxation) can be strongly influenced by the packing efficiency of molecules, which is tied to their structural flexibility (configurational entropy). However, the molecular shape, while producing strong packing anisotropy in PVD glasses, appears to be unimportant in the glass stability.

Molecular layering, while ubiquitous, had not previously been considered as a critical structural property. We present strong evidence that the deposition temperature below which layering is observed in GIWAXS experiments, can be used as a strong proxy for the glass transition temperature of the surface layer, and the strength of layering can be attributed to the rate of surface-mediated accelerated aging (SMA) at a given deposition rate and temperature.

ACKNOWLEDGEMENTS

This work was funded by NSF-DMR grant (DMREF-1628407), and partially by NSF-Materials Research Science and Engineering Centers (MRSEC) DMR-1720530. The authors acknowledge the use of the Dual Source and Environmental X-ray Scattering facility operated by the Labo-

ratory for Research on the Structure of Matter at the University of Pennsylvania (NSF-MRSEC DMR-1720530) and Prof. Paul Heiney. The equipment purchase was made possible by an NSF Major Research Instrumentation Program (MRI) grant (NSF-17-25969), an Army Research Office (ARO) Defense University Research Instrumentation Program (DURIP) grant (W911NF-17-1-0282), and the University of Pennsylvania. ARM and RAR gratefully acknowledge computational resources provided through XSEDE award TG-DMR150034. The authors acknowledge the National Synchrotron Light Source II (NSLS-II) at the Brookhaven National Lab (BNL) and BNL scientists Mikhail Zhernenkovc and Guillaume Freychetc for their help in obtaining the data in Figure S9. PJW thanks support from the NSF grant CHE-1902509. We thank Dr. Jun Gu, Dr. and Chad W. Lawrence for their helpful discussions on measurements of rotational barriers in molecular glasses.

Author Contributions: Aixi Zhang and Sarah Wolf performed vapor depositions. Alex Moore performed molecular dynamics simulations. Haoqiang Zhao synthesized the compounds and Shivajee Govind performed NMR measurements. Aixi Zhang, Shivajee Govind, and Yi Jin performed characterization experiments. Aixi Zhang, Sarah Wolf, Shivajee Govind, and Alex R. Moore performed data analysis. Aixi Zhang, Alex R. Moore, Robert A. Riggleman, Patrick J. Walsh and Zahra Fakhraai conceptualized the ideas. Aixi Zhang, Alex R. Moore, and Zahra Fakhraai wrote the article. Zahra Fakhraai directed the research.

Conflict of Interest: The authors have no conflict of interest to declare.

REFERENCES

¹S. F. Swallen, K. L. Kearns, M. K. Mapes, Y. S. Kim, R. J. McMahon, M. D. Ediger, T. Wu, L. Yu, and S. Satija, "Organic glasses with exceptional thermodynamic and kinetic stability," Science **315**, 353–356 (2007).

²K. L. Kearns, S. F. Swallen, M. D. Ediger, T. Wu, Y. Sun, and L. Yu, "Hiking down the energy landscape: progress toward the kauzmann temperature via vapor deposition," The Journal of Physical Chemistry B **112**, 4934–4942 (2008).

³T. Liu, K. Cheng, E. Salami-Ranjbaran, F. Gao, C. Li, X. Tong, Y.-C. Lin, Y. Zhang, W. Zhang, L. Klinge, P. J. Walsh, and Z. Fakhraai, "The effect of chemical structure on the stability of physical vapor deposited glasses of 1,3,5-triarylbenzene," The Journal of Chemical Physics **143**, 084506 (2015).

- ⁴J. Ràfols-Ribé, M. Gonzalez-Silveira, C. Rodríguez-Tinoco, and J. Rodríguez-Viejo, "The role of thermodynamic stability in the characteristics of the devitrification front of vapour-deposited glasses of toluene," Physical Chemistry Chemical Physics **19**, 11089–11097 (2017).
- ⁵A. Laventure, A. Gujral, O. Lebel, C. Pellerin, and M. D. Ediger, "Influence of hydrogen bonding on the kinetic stability of vapor-deposited glasses of triazine derivatives," The Journal of Physical Chemistry B **121**, 2350–2358 (2017).
- ⁶S. S. Dalal and M. D. Ediger, "Molecular orientation in stable glasses of indomethacin," The Journal of Physical Chemistry Letters **3**, 1229–1233 (2012).
- ⁷D. M. Walters, R. Richert, and M. D. Ediger, "Thermal stability of vapor-deposited stable glasses of an organic semiconductor," The Journal of Chemical Physics **142**, 134504 (2015).
- ⁸J. Ràfols-Ribé, A. Vila-Costa, C. Rodríguez-Tinoco, A. F. Lopeandía, J. Rodríguez-Viejo, and M. Gonzalez-Silveira, "Kinetic arrest of front transformation to gain access to the bulk glass transition in ultrathin films of vapour-deposited glasses," Physical Chemistry Chemical Physics **20**, 29989–29995 (2018).
- ⁹D. Yokoyama, "Molecular orientation in small-molecule organic light-emitting diodes," Journal of Materials Chemistry **21**, 19187 (2011).
- ¹⁰S. S. Dalal, D. M. Walters, I. Lyubimov, J. J. de Pablo, and M. D. Ediger, "Tunable molecular orientation and elevated thermal stability of vapor-deposited organic semiconductors," Proceedings of the National Academy of Sciences **112**, 4227–4232 (2015).
- ¹¹M. Shibata, Y. Sakai, and D. Yokoyama, "Advantages and disadvantages of vacuum-deposited and spin-coated amorphous organic semiconductor films for organic light-emitting diodes," Journal of Materials Chemistry C 3, 11178–11191 (2015).
- ¹²D. M. Walters, L. Antony, J. J. de Pablo, and M. D. Ediger, "Influence of molecular shape on the thermal stability and molecular orientation of vapor-deposited organic semiconductors," The Journal of Physical Chemistry Letters **8**, 3380–3386 (2017).
- ¹³M. Oh-e, H. Ogata, and F. Araoka, "Randomization and constraint of molecular alignment and orientation: Temperature-dependent anisotropy and phase transition in vapor-deposited thin films of an organic cross-shaped molecule," ACS Omega **4**, 39–47 (2019).
- ¹⁴A. Mikaeili, T. Matsushima, Y. Esaki, S. A. Yazdani, C. Adachi, and E. Mohajerani, "The origin of changes in electrical properties of organic films fabricated at various vacuum-deposition rates," Optical Materials **91**, 93–100 (2019).

- ¹⁵F. Hellman, "Surface-induced ordering: A model for vapor-deposition growth of amorphous materials," Applied Physics Letters **64**, 1947–1949 (1994).
- ¹⁶K. J. Dawson, L. Zhu, L. Yu, and M. D. Ediger, "Anisotropic structure and transformation kinetics of vapor-deposited indomethacin glasses," The Journal of Physical Chemistry B **115**, 455–463 (2011).
- ¹⁷D. Yokoyama, Y. Setoguchi, A. Sakaguchi, M. Suzuki, and C. Adachi, "Orientation control of linear-shaped molecules in vacuum-deposited organic amorphous films and its effect on carrier mobilities," Advanced Functional Materials **20**, 386–391 (2010).
- ¹⁸A. Gujral, K. A. O'Hara, M. F. Toney, M. L. Chabinyc, and M. Ediger, "Structural characterization of vapor-deposited glasses of an organic hole transport material with x-ray scattering," Chemistry of Materials **27**, 3341–3348 (2015).
- ¹⁹A. Gujral, L. Yu, and M. Ediger, "Anisotropic organic glasses," Current Opinion in Solid State and Materials Science (2017), 10.1016/j.cossms.2017.11.001.
- ²⁰K. Bagchi, A. Gujral, M. F. Toney, and M. D. Ediger, "Generic packing motifs in vapor-deposited glasses of organic semiconductors," Soft Matter **15**, 7590–7595 (2019).
- ²¹X. Xing, L. Zhong, L. Zhang, Z. Chen, B. Qu, E. Chen, L. Xiao, and Q. Gong, "Essential differences of organic films at the molecular level via vacuum deposition and solution processes for organic light-emitting diodes," The Journal of Physical Chemistry C **117**, 25405–25408 (2013).
- ²²S. Sohn, K. H. Park, S.-K. Kwon, H.-K. Lee, H. Ahn, S. Jung, and Y.-H. Kim, "Preferential orientation of tetrahedral silicon-based hosts in phosphorescent organic light-emitting diodes," ACS Omega 3, 9989–9996 (2018).
- ²³T. Liu, A. L. Exarhos, E. C. Alguire, F. Gao, E. Salami-Ranjbaran, K. Cheng, T. Jia, J. E. Subotnik, P. J. Walsh, J. M. Kikkawa, and Z. Fakhraai, "Birefringent stable glass with predominantly isotropic molecular orientation," Physical Review Letters 119 (2017), 10.1103/physrevlett.119.095502.
- ²⁴Y. Noguchi, Y. Miyazaki, Y. Tanaka, N. Sato, Y. Nakayama, T. D. Schmidt, W. Brütting, and H. Ishii, "Charge accumulation at organic semiconductor interfaces due to a permanent dipole moment and its orientational order in bilayer devices," Journal of Applied Physics 111, 114508 (2012).
- ²⁵Z. Fakhraai, T. Still, G. Fytas, and M. D. Ediger, "Structural variations of an organic glassformer vapor-deposited onto a temperature gradient stage," The Journal of Physical Chemistry Letters 2, 423–427 (2011).

- ²⁶S. E. Wolf, S. Fulco, A. Zhang, H. Zhao, P. J. Walsh, K. T. Turner, and Z. Fakhraai, "Role of molecular layering in the enhanced mechanical properties of stable glasses," The Journal of Physical Chemistry Letters **13**, 3360–3368 (2022).
- ²⁷J. M. Torres, N. Bakken, J. Li, and B. D. Vogt, "Substrate temperature to control moduli and water uptake in thin films of vapor deposited n,n/-di(1-naphthyl)-n,n/-diphenyl-(1,1/-biphenyl)-4,4/-diamine (NPD)," The Journal of Physical Chemistry B **119**, 11928–11934 (2015).
- ²⁸C. Tangpatjaroen, K. Bagchi, R. A. Martínez, D. Grierson, and I. Szlufarska, "Mechanical properties of structure-tunable, vapor-deposited TPD glass," The Journal of Physical Chemistry C **122**, 27775–27781 (2018).
- ²⁹Y. Esaki, T. Komino, T. Matsushima, and C. Adachi, "Enhanced electrical properties and air stability of amorphous organic thin films by engineering film density," The Journal of Physical Chemistry Letters **8**, 5891–5897 (2017).
- ³⁰K. Bagchi and M. D. Ediger, "Controlling structure and properties of vapor-deposited glasses of organic semiconductors: Recent advances and challenges," The Journal of Physical Chemistry Letters **11**, 6935–6945 (2020).
- ³¹C. Bishop, J. L. Thelen, E. Gann, M. F. Toney, L. Yu, D. M. DeLongchamp, and M. D. Ediger, "Vapor deposition of a nonmesogen prepares highly structured organic glasses," Proceedings of the National Academy of Sciences, 201908445 (2019).
- ³²K. Bagchi, N. E. Jackson, A. Gujral, C. Huang, M. F. Toney, L. Yu, J. J. de Pablo, and M. D. Ediger, "Origin of anisotropic molecular packing in vapor-deposited alq3 glasses," The Journal of Physical Chemistry Letters, 164–170 (2018).
- ³³S. S. Dalal, A. Sepúlveda, G. K. Pribil, Z. Fakhraai, and M. D. Ediger, "Density and birefringence of a highly stable α, α, β -trisnaphthylbenzene glass," The Journal of Chemical Physics **136**, 204501 (2012).
- ³⁴T. J. Ferron, J. L. Thelen, K. Bagchi, C. Deng, E. Gann, J. J. de Pablo, M. Ediger, D. F. Sunday, and D. M. DeLongchamp, "Characterization of the interfacial orientation and molecular conformation in a glass-forming organic semiconductor," ACS Applied Materials & Interfaces (2022).
- ³⁵C. Bishop, Y. Li, M. F. Toney, L. Yu, and M. D. Ediger, "Molecular orientation for vapor-deposited organic glasses follows rate-temperature superposition: The case of posaconazole," The Journal of Physical Chemistry B 124, 2505–2513 (2020).

- ³⁶I. Lyubimov, L. Antony, D. M. Walters, D. Rodney, M. D. Ediger, and J. J. de Pablo, "Orientational anisotropy in simulated vapor-deposited molecular glasses," The Journal of Chemical Physics **143**, 094502 (2015).
- ³⁷E. Thoms, J. P. Gabriel, A. Guiseppi-Elie, M. D. Ediger, and R. Richert, "In situ observation of fast surface dynamics during the vapor-deposition of a stable organic glass," Soft Matter (2020), 10.1039/d0sm01916j.
- ³⁸J. L. Thelen, C. Bishop, K. Bagchi, D. F. Sunday, E. Gann, S. Mukherjee, L. J. Richter, R. J. Kline, M. D. Ediger, and D. M. DeLongchamp, "Molecular orientation depth profiles in organic glasses using polarized resonant soft x-ray reflectivity," Chemistry of Materials **32**, 6295–6309 (2020).
- ³⁹A. R. Moore, G. Huang, S. Wolf, P. J. Walsh, Z. Fakhraai, and R. A. Riggleman, "Effects of microstructure formation on the stability of vapor-deposited glasses," Proceedings of the National Academy of Sciences **116**, 5937–5942 (2019).
- ⁴⁰L. Berthier, P. Charbonneau, E. Flenner, and F. Zamponi, "Origin of ultrastability in vapor-deposited glasses," Physical Review Letters **119** (2017), 10.1103/physrevlett.119.188002.
- ⁴¹L. Yu, "Surface mobility of molecular glasses and its importance in physical stability," Advanced Drug Delivery Reviews **100**, 3–9 (2016).
- ⁴²Y. Zhang and Z. Fakhraai, "Decoupling of surface diffusion and relaxation dynamics of molecular glasses," Proceedings of the National Academy of Sciences **114**, 4915–4919 (2017).
- ⁴³D. M. Sussman, S. S. Schoenholz, E. D. Cubuk, and A. J. Liu, "Disconnecting structure and dynamics in glassy thin films," Proceedings of the National Academy of Sciences **114**, 10601–10605 (2017).
- ⁴⁴Y. Zhang, E. C. Glor, M. Li, T. Liu, K. Wahid, W. Zhang, R. A. Riggleman, and Z. Fakhraai, "Long-range correlated dynamics in ultra-thin molecular glass films," The Journal of Chemical Physics **145**, 114502 (2016).
- ⁴⁵W. Zhang, C. W. Brian, and L. Yu, "Fast surface diffusion of amorphouso-terphenyl and its competition with viscous flow in surface evolution," The Journal of Physical Chemistry B **119**, 5071–5078 (2015).
- ⁴⁶C. Rodríguez-Tinoco, M. Gonzalez-Silveira, J. Ràfols-Ribé, A. Vila-Costa, J. C. Martinez-Garcia, and J. Rodríguez-Viejo, "Surface-bulk interplay in vapor-deposited glasses: Crossover length and the origin of front transformation," Physical review letters **123**, 155501 (2019).

- ⁴⁷Y. Zhang and Z. Fakhraai, "Invariant fast diffusion on the surfaces of ultrastable and aged molecular glasses," Physical Review Letters **118** (2017), 10.1103/physrevlett.118.066101.
- ⁴⁸A. Sepúlveda, E. Leon-Gutierrez, M. Gonzalez-Silveira, C. Rodríguez-Tinoco, M. Clavaguera-Mora, and J. Rodriguez-Viejo, "Accelerated aging in ultrathin films of a molecular glass former," Physical review letters **107**, 025901 (2011).
- ⁴⁹S. Samanta, G. Huang, G. Gao, Y. Zhang, A. Zhang, S. Wolf, C. N. Woods, Y. Jin, P. J. Walsh, and Z. Fakhraai, "Exploring the importance of surface diffusion in stability of vapor-deposited organic glasses," The Journal of Physical Chemistry B **123**, 4108–4117 (2019).
- ⁵⁰C. W. Brian and L. Yu, "Surface self-diffusion of organic glasses," The Journal of Physical Chemistry A **117**, 13303–13309 (2013).
- ⁵¹Y. Chua, M. Ahrenberg, M. Tylinski, M. Ediger, and C. Schick, "How much time is needed to form a kinetically stable glass? ac calorimetric study of vapor-deposited glasses of ethylcyclohexane," The Journal of chemical physics **142**, 054506 (2015).
- ⁵²D. Chatterjee, A. Annamareddy, J. Ketkaew, J. Schroers, D. Morgan, and P. M. Voyles, "Fast surface dynamics on a metallic glass nanowire," ACS nano **15**, 11309–11316 (2021).
- ⁵³K. Paeng, S. F. Swallen, and M. D. Ediger, "Direct measurement of molecular motion in free-standing polystyrene thin films," Journal of the American Chemical Society **133**, 8444–8447 (2011).
- ⁵⁴J. Teichroeb and J. Forrest, "Direct imaging of nanoparticle embedding to probe viscoelasticity of polymer surfaces," Physical review letters **91**, 016104 (2003).
- ⁵⁵D. Qi, M. Ilton, and J. Forrest, "Measuring surface and bulk relaxation in glassy polymers," The European Physical Journal E **34**, 1–7 (2011).
- ⁵⁶K. Bagchi, C. Deng, C. Bishop, Y. Li, N. E. Jackson, L. Yu, M. Toney, J. De Pablo, and M. Ediger, "Over what length scale does an inorganic substrate perturb the structure of a glassy organic semiconductor?" ACS applied materials & interfaces **12**, 26717–26726 (2020).
- ⁵⁷T. Liu, K. Cheng, E. Salami-Ranjbaran, F. Gao, E. C. Glor, M. Li, P. J. Walsh, and Z. Fakhraai, "Synthesis and high-throughput characterization of structural analogues of molecular glassformers: 1,3,5-trisarylbenzenes," Soft Matter **11**, 7558–7566 (2015).
- ⁵⁸S. E. Wolf, T. Liu, S. Govind, H. Zhao, G. Huang, A. Zhang, Y. Wu, J. Chin, K. Cheng, E. Salami-Ranjbaran, *et al.*, "Design of a homologous series of molecular glassformers," J. Chem. Phys. **155**, 224503 (2021).

- ⁵⁹Y. Jin, A. Zhang, S. E. Wolf, S. Govind, A. R. Moore, M. Zhernenkov, G. Freychet, A. A. Shamsabadi, and Z. Fakhraai, "Glasses denser than the supercooled liquid," Proceedings of the National Academy of Sciences **118** (2021).
- ⁶⁰A. Zhang, *Manipulating Glass Structure and Properties Through Surface Mediated Equilibrium*, Ph.D. thesis, University of Pennsylvania (2021).
- ⁶¹K. Nikitin, H. Müller-Bunz, Y. Ortin, J. Muldoon, and M. J. McGlinchey, "Restricted rotation in 9-phenyl-anthracenes: A prediction fulfilled," Organic Letters **13**, 256–259 (2011).
- ⁶²D. Nori-shargh, S. Asadzadeh, F.-R. Ghanizadeh, F. Deyhimi, M. M. Amini, and S. Jameh-Bozorghi, "Ab initio study of the structures and dynamic stereochemistry of biaryls," Journal of Molecular Structure: THEOCHEM **717**, 41–51 (2005).
- ⁶³S. Singh and J. J. de Pablo, "A molecular view of vapor deposited glasses," The Journal of chemical physics **134**, 194903 (2011).
- ⁶⁴S. Plimpton, "Fast parallel algorithms for short-range molecular dynamics," Journal of Computational Physics **117**, 1–19 (1995).
- ⁶⁵F. Varnik, J. Baschnagel, and K. Binder, "Reduction of the glass transition temperature in polymer films: A molecular-dynamics study," Physical Review E 65, 021507 (2002).
- ⁶⁶G. Sun, S. Saw, I. Douglass, and P. Harrowell, "Structural origin of enhanced dynamics at the surface of a glassy alloy," Physical Review Letters **119**, 245501 (2017).
- ⁶⁷Y. Zhang, C. N. Woods, M. Alvarez, Y. Jin, R. A. Riggleman, and Z. Fakhraai, "Effect of substrate interactions on the glass transition and length-scale of correlated dynamics in ultra-thin molecular glass films," The Journal of Chemical Physics **149**, 184902 (2018).
- ⁶⁸S. S. Dalal, Z. Fakhraai, and M. D. Ediger, "High-throughput ellipsometric characterization of vapor-deposited indomethacin glasses," The Journal of Physical Chemistry B **117**, 15415–15425 (2013).
- ⁶⁹J. H. Mangalara, M. D. Marvin, and D. S. Simmons, "Three-layer model for the emergence of ultrastable glasses from the surfaces of supercooled liquids," The Journal of Physical Chemistry B **120**, 4861–4865 (2016).